Journal of Autoimmunity 140 (2023) 103094

Contents lists available at ScienceDirect

Journal of Autoimmunity

journal homepage: www.elsevier.com/locate/jautimm

Harnessing autoimmunity with dominant self-peptide: Modulating the sustainability of tissue-preferential antigen-specific Tregs by governing the binding stability via peptide flanking residues

Youwei Lin [a,b,*], Shun Sakuraba [c], Chandirasegaran Massilamany [d], Jayagopala Reddy [e], Yoshimasa Tanaka [f], Sachiko Miyake [g], Takashi Yamamura [a,**]

[a] Department of Immunology, National Institute of Neuroscience, National Center of Neurology and Psychiatry, Tokyo, 187-8502, Japan
[b] Department of Neurology, National Center Hospital, National Center of Neurology and Psychiatry, Tokyo, 187-8551, Japan
[c] National Institutes for Quantum Science and Technology, Institute for Quantum Life Science, Chiba, 263-0024, Japan
[d] Immuno-oncology CRISPR Therapeutics, Boston, MA, 02127, USA
[e] School of Veterinary Medicine and Biomedical Sciences, University of Nebraska-Lincoln, Lincoln, NE, 68583, USA
[f] Center for Medical Innovation, Nagasaki University, Nagasaki, 852-8588, Japan
[g] Department of Immunology, Juntendo University School of Medicine, Tokyo, 113-8421, Japan

ARTICLE INFO

Handling Editor: M.E. Gershwin

Keywords:
Experimental autoimmune encephalomyelitis
Dominant self-peptide
Regulatory T-cell
Antigen specificity
Peptide flanking residue
Binding stability

ABSTRACT

Sensitization to self-peptides induces various immunological responses, from autoimmunity to tumor immunity, depending on the peptide sequence; however, the underlying mechanisms remain unclear, and thus, curative therapeutic options considering immunity balance are limited. Herein, two overlapping dominant peptides of myelin proteolipid protein, PLP136-150 and PLP139-151, which induce different forms of experimental autoimmune encephalomyelitis (EAE), monophasic and relapsing EAE, respectively, were investigated. Mice with monophasic EAE exhibited highly resistant to EAE re-induction with any encephalitogenic peptides, whereas mice with relapsing EAE were susceptible, and progressed, to EAE re-induction. This resistance to relapse and re-induction in monophasic EAE mice was associated with the maintenance of potent $CD69^{+}CD103^{+}CD4^{+}CD25^{high}$ regulatory T-cells (Tregs) enriched with antigen specificity, which expanded preferentially in the central nervous system with sustained suppressive activity. This tissue-preferential sustainability of potent antigen-specific Tregs was correlated with the antigenicity of PLP136-150, depending on its flanking residues. That is, the flanking residues of PLP136-150 enable to form pivotally arranged strong hydrogen bonds that secured its binding stability to MHC-class II. These potent Tregs acting tissue-preferentially were induced only by sensitization of PLP136-150, not by its tolerance induction, independent of EAE development. These findings suggest that, for optimal therapy, "benign autoimmunity" can be critically achieved through inverse vaccination with self-peptides by manipulating their flanking residues.

1. Introduction

Host immune systems, crucial for maintaining physiological homeostasis and enabling host protection against exogenous and endogenous insults, can discriminate between self and non-self to provoke potent responses against foreign microbial antigens while avoiding self-antigens. Self/non-self discrimination depends on a finely tuned balance of inflammatory effectors and protective regulators [1,2]. Sensitization to self-antigens may cause autoimmune reactions, which can be benign or hazardous to human health [3,4]. The clinical manifestation and course of autoimmune diseases vary greatly between individuals [5]; however, the precise mechanisms that enable self-antigens to elicit such a wide diversity of effects on multiple immune constituents remain unclear. This lack of mechanistic insight has limited the selection of optimal self-peptide ligands for designing autoimmune disease and tumor immunotherapies [6,7]. Indeed, the immunotherapies that have

* Corresponding author. Department of Immunology, National Institute of Neuroscience, National Center of Neurology and Psychiatry, Tokyo, 187-8502, Japan.
** Corresponding author.
E-mail addresses: lin@ncnp.go.jp (Y. Lin), sakuraba.shun@qst.go.jp (S. Sakuraba), mchandirasegaran@gmail.com (C. Massilamany), jayreddy@unl.edu (J. Reddy), ystanaka@nagasaki-u.ac.jp (Y. Tanaka), s-miyake@juntendo.ac.jp (S. Miyake), yamamura@ncnp.go.jp (T. Yamamura).

https://doi.org/10.1016/j.jaut.2023.103094
Received 25 May 2023; Received in revised form 21 July 2023; Accepted 25 July 2023
Available online 14 September 2023

been developed specifically target single key cells and molecules without sufficiently considering disease-related antigens [7–9]. Moreover, although these advanced therapies can dramatically mitigate the disease state and thus lead to clinical breakthroughs, their therapeutic efficacies vary depending on the disease types, even if they share the same target. They also fail to fully inhibit disease activity or attenuate disease progression due to the presence of several disease targets, even by combination therapy [7]. Furthermore, severe adverse reactions may develop, including infection, tumors and other autoimmune diseases, due to their extrinsic over-suppression via the collateral immune disequilibrium [8–10]. Several promising antigen-based approaches have been investigated to address these challenges; however, none have exhibited curative effects [7,11–14], while others reportedly exacerbate certain conditions [7,11]. Elucidation of the underlying mechanisms guiding the kinetics of autoimmune reactions to self-antigen peptides could enhance the efficacy and optimal use of selective therapeutics.

Experimental autoimmune encephalomyelitis (EAE) is widely employed to study the induction and regulation of autoimmune responses [15]. This animal model is induced by administrating central nervous system (CNS) components mixed with an adjuvant [16–18], mediated by encephalitogenic $CD4^+$ T-cells [19]. Recent studies have suggested that CNS components also induce $CD8^+$ T cells and contribute to the development of EAE [20,21]. EAE serves as a representative animal model of multiple sclerosis (MS), an autoimmune disease affecting the CNS [22], and exhibits significant diversity in its clinical course, like human MS, ranging from monophasic (M-EAE) to relapsing-remitting (RR-EAE) and progressive forms [23]. This heterogeneity in the clinical phenotype is partially explained by the genetic background of mice [24–26], which includes non-MHC genes controlling EAE susceptibility [27] and MHC-class II genes defining the corresponding encephalitogenic epitopes [23,25–29]. It is, therefore, theoretically impossible to reflect different courses of EAE in one strain without cross-breeding or protocol changes [15,24,25].

Herein, we investigated how sensitization to individual self-antigen peptides yields discrete immune responses, leading to either disease initiation or disease prevention in EAE models. From the observation that two overlapping peptides can induce M-EAE and RR-EAE in SJL/J mice, we hypothesized that the differences in relapse susceptibility between these EAEs are due to differences in their functional and structural aspects. Functionally, the potent regulatory T-cells (Tregs) might exhibit different kinetics and antigen specificity, which might be preferentially sustained in the CNS tissue. Additionally, the structural differences in the flanking residues outside the MHC groove between the sensitized overlapping peptides could influence their binding ability to the MHC-class II molecules and determine their antigen specificity. The findings of this study have implications for the development of novel antigen-based therapies that can be used to control the sustainability of antigen-specific Tregs in target tissue by manipulating the self-antigen peptide flanking residues, which may significantly influence autoimmunity regulation.

2. Materials and methods

2.1. Mice

Female SJL/J mice (5–7-week-old) were purchased from Charles River Laboratory (Tokyo, Japan) and housed under specific pathogen-free conditions in accordance with institutional guidelines. All animal protocols were approved by the Animal Ethics Committee of the National Institute of Neuroscience, National Center of Neurology and Psychiatry (NCNP), Japan (approval number 2007037, 2011015, 2014011, and 2020008).

2.2. Peptides

Murine PLP, MBP, and MOG peptides were synthesized by automated Fmoc solid-phase peptide synthesis at Toray Laboratories (Tokyo, Japan) as follows: PLP136-150, RVSHSLGKWLGHPDK [30]; PLP139-151, HSLGKWLGHPDKF [28]; PLP178-191, NTWTTCQSIAFPSK [31]; MBP89-101, VHFFKNIVTPRTP [32]; MOG92-106, DEGGYTCFFRDHSYQ [33]. C138 and C140 in PLP136-150 were mutated to S to avoid C–C disulfide bridging. C140 in PLP139-151 was also substituted with S as described previously [28], which certainly did not change the results of EAE (data not shown). Type II collagen peptide (bovine) was synthesized at the Collagen Research Center (Tokyo, Japan) while ovalbumin peptide (OVA 323–339) was synthesized at Peptide Institute Inc. (Osaka, Japan).

2.3. EAE induction

EAE (active EAE) was induced in 6–8-week-old female mice via subcutaneous immunization in the tail base bilaterally with 100 μg PLP-peptide in 100 μL of PBS in an emulsion mixed with 100 μL of incomplete Freund's adjuvant (IFA; Difco, Detroit, USA) supplemented with 1 mg *Mycobacterium tuberculosis* H37Ra (Difco, Detroit, USA) as described previously [34]. The mice were then immediately injected intraperitoneally with 200 ng pertussis toxin (PT; List Biological Laboratories, Campbell, USA); the injection was repeated after two days. The secondary challenge for EAE (re-induction [35]) was introduced similarly on d35. Mice were examined daily for clinical signs of EAE and scored as follows [36]: 0 = normal; 1 = loss of tail tonicity; 2 = partial hind limb paresis; 3 = complete hind limb paralysis; 4 = hind limb paralysis with body paresis; 5 = hind- and forelimb paresis; 6 = death.

Passive EAE was induced in 6–8-week-old irradiated (300-rad) female mice via intraperitoneal administration of peptide-primed lymph node (LN) cells at 1.0×10^7/mouse. Peptide-primed LN cells were prepared by immunizing the cells with 100 μg PLP-peptide and incubating the day 10–11 primed cells with the priming peptide for three days [36].

2.4. CIA induction

To induce collagen-induced arthritis (CIA), 100 μg bovine type II collagen dissolved in 100 μL of PBS was emulsified with an equal volume of complete Freund's adjuvant (CFA; Difco, Detroit, USA) supplemented with 250 μg M. *tuberculosis* H37Ra. Then 200 μL of the emulsion was inoculated intradermally (id) into the tail base at day 0 and boosted at day 21. Disease severity of CIA was determined as a summation of the scores for each limb evaluated as follows: 0 = no change; 1 = focal erythema of the limb; 2 = mild swelling and erythema of the limb; 3 = pronounced swelling and erythema of the limb; 4 = maximum swelling and erythema of the limb with joint deformity. The cumulative score was calculated by summing up the daily scores of each mouse [37].

2.5. Recall response to encephalitogenic peptide and evaluation of cytokine production

To evaluate the recall response to several peptides, we immunized the mice with each peptide without administering PT. At various time points, we prepared single-cell suspensions of draining LN and spleen cells by mechanical disruption in standard media (RPMI 1640 supplemented with 5.5×10^{-5} M 2-mercaptoethanol, 2 mM L-glutamine, 100 U/mL penicillin and streptomycin) supplemented with 1% syngeneic mouse serum. Cell suspensions were cultured with varying concentrations of PLP-peptides in 96-well flat-bottom microwell plates at 1×10^6/200 μL/well for 72 h. T-cell proliferation was determined by measuring [^{3}H]-thymidine (1 μCi/well) incorporation in the final 24 h of the culture. The capability of cells to produce IFNγ and IL-17 was also evaluated by collecting culture supernatant before [^{3}H]-thymidine labeling and analyzing cytokine levels via ELISA, as described previously [34].

2.6. Adoptive transfer of primed cells

Either total LN cells (3.0×10^7/mouse) or LN subpopulations ($CD4^-$ and $CD4^+CD25^-$ cells; both 1.0×10^7/mice and $CD4^+CD25^+$ cells: 1.0×10^5/mouse) from PLP136-150- or PLP139-151-primed cells obtained by mechanical disruption were suspended in 200 μL of PBS and intraperitoneally administered to naïve mice, which were then induced EAE with PLP139-151 five days later.

2.7. Flow cytometry

To characterize the heterogeneity of the $CD4^+CD25^+$ T-cells, they were stained with the following monoclonal antibodies in the presence of FcγRII/III antibody (CD16/32): perCP-*anti*-CD4 (L3T4), PE-*anti*-CD25 (PC61), FITC- or biotin-*anti*-CD69 (H1·2F3), FITC- or biotin-*anti*-CD103 (M290) (BD PharMingen, San Diego, USA), and FITC- or APC-*anti*-Foxp3 (FJK-16 S) (eBioscience, San Diego, USA). Biotinylated cells were conjugated with streptavidin-APC, and samples were analyzed on a FACSCalibur system using CellQuest (Becton Dickinson, Franklin Lakes, USA) and FlowJo (Tomy Digital Biology Co., Ltd., Tokyo, Japan). To determine the T-cell frequency (total, $CD4^+$ or $CD8^+$) and B-cells, perCP-*anti*-CD3 (2C11), PE-*anti*-CD4 (L3T4), FITC-*anti*-CD8a (Ly-2), and perCP-*anti*-CD19 (1D3) (BD PharMingen, San Diego, USA) were used.

2.8. Depletion of $CD25^+$ cells

An anti-CD25 mAb was purified from ascites fluid of ICR nude mice inoculated with PC61 hybridoma using a protein G column (Cosmo Bio Co., Ltd., Tokyo, Japan) and intraperitoneally (ip) injected at 500 μg/mouse five days before EAE induction.

2.9. Isolation of subpopulations among $CD4^+CD25^+$ T-cells

$CD4^+CD25^+$ T-cell subpopulations ($CD69^+CD103^+$, $CD69^+CD103^-$, $CD69^-CD103^+$ and $CD69^-CD103^-$) subpopulations were obtained by $CD4^+CD25^+$ T-cell isolation using a $CD4^+CD25^+$ Regulatory T-cell Isolation Kit (Miltenyi Biotec, Bergisch Gladbach, Germany), subsequently stained with a combination of FITC-*anti*-CD69 and biotin-*anti*-CD103, or biotin-*anti*-CD69 and FITC-*anti*-CD103, and reacted with streptavidin-APC. Alternatively, the $CD4^+CD25^+$ T-cells were isolated using biotin *anti*-CD25 after isolation of $CD4^+$ T-cells using a CD4 Isolation Kit (Miltenyi Biotec, Bergisch Gladbach, Germany) and subsequently staining them with perCP-*anti*-CD69 and FITC-*anti*-CD103. The cells were sorted using an EPICS ALTRA (Beckman Coulter, Fullerton, CA) or BD FACS Aria II (Becton Dickinson, Franklin Lakes, USA) system.

2.10. Evaluation of in vitro and in vivo suppressive capacity of $CD4^+CD25^+$ T-cells

To evaluate the *in vitro* suppressive activity of sorted subpopulations of $CD4^+CD25^+$ T-cells primed with either of the PLP-peptides, LN cells from day 14 PLP139-151-primed mice were used as effector cells and stimulated with PLP139-151 (100 μg/mL) in the presence of each subpopulation in 96-well U-bottom plates for 96 h. Cellular proliferation was measured as previously described. The cultures comprised a fixed number of LN cells (5×10^5/well) and the sorted subpopulation at a ratio of 20:1, 10:1, or 5:1 as well as irradiated splenocytes from naïve mice as feeder cells (0.5×10^6/well). The *in vitro* suppressive activity was also measured via flow cytometry by evaluating the proliferation of CFSE-labeled effector cells as the $CFSE^{low}$ population, according to the procedure described by eBioscience (San Diego, USA). The *in vivo* suppressive activity was evaluated by intraperitoneal administration of sorted subpopulations of $CD4^+CD25^+$ T-cells and total $CD4^+CD25^+$ T-cells derived from PLP136-150-immunized mice (1×10^5/mice of each) into naïve mice before EAE induction by challenge with PLP139-151 five days later.

2.11. Evaluation of antigen specificity in PLP-peptide-primed cells and their subpopulations

Experiments were performed as previously described [38,39]. Briefly, $CD4^+$ and $CD4^+CD25^+$ T-cells were isolated using the $CD4^+$ T-cell Isolation Kit or $CD4^+CD25^+$ Regulatory T-cell Isolation Kit (Miltenyi Biotec, Bergisch Gladbach, Germany) from PLP-peptide-primed LN cells and their sorted subpopulations were stimulated with both PLP-peptides and irradiated splenocytes used as antigen-presenting cells at 37 °C for four days. The stimulated cells were then stained with I–As dextramer in the presence of IL-2. Under resting conditions, the stimulation with the priming peptide was omitted. Under activating conditions, we determined the $dextramer^+$ population in the lymphocyte and lymphoblast areas demarcated on the scatter plot (the population with a larger Forward Scatter [FSC] than lymphocytes was demarcated as lymphoblasts).

2.12. Peptide-specific tolerance induction

We adopted three protocols to obtain peptide-specific tolerance: 'peptide/IFA ip,' 'high-dose peptide iv,' and 'peptide-coupled with splenocyte iv.' 'Peptide/IFA ip' was induced 14 days before EAE induction by intraperitoneal administration of 300 μg of peptide dissolved in PBS in an emulsion mixed with incomplete Freund's adjuvant (IFA; Difco, Detroit, USA) [40]. 'High-dose peptide iv' was induced 10 days before EAE induction by intravenous administration of 300 μg of peptide dissolved in PBS [41]. 'Peptide-coupled with splenocyte iv' was induced seven days before EAE induction by intravenous administration of 5×10^6 naïve splenocytes conjugated with each peptide at 1 mg/mL and 150 mg/mL 1-(3-dimethylaminopropyl)-3-ethylcarbodiimide (EDAC; CalBioChem, LaJolla, CA, USA) [42].

2.13. Peptide binding stability evaluation

2.13.1. Modeling mouse MHC-class II (I–As)–PLP complexes

Three-dimensional models of mouse MHC-class II (I–As)−PLP complexes were created based on a mouse MHC-class II (I-Ax)−peptide complex (PDBID: 1IAK) as a template using HOMCOS [43] and MODELLER [44] software packages. After the structures were refined by MD simulation, all-atom, explicit-solvent models of complexes I–As with PLP136-150 and I–As with PLP139-151 were constructed using the homology-modeled structures. Both models were solvated in 0.15 M sodium chloride solution. To represent an interaction potential function, we used the AMBER14SB force field [45], TIP3P [46], and Joung--Cheatham's monovalent ion parameters [47]. The model was relaxed with 1000 steps of energy minimization and a 1 ns of equilibration run under a 300 K and 1 atm (NPT) condition.

2.13.2. Molecular dynamics simulation of I–As–PLP complexes

Replica Exchange with Solute Tempering 2 (REST2) [48] simulation was employed to relax the initial model, and representative structures were extracted from the trajectories of the PLP-MHC complexes. Generally, configurations sampled from simulations with REST2 converge to a true distribution faster than those with conventional MD simulation under the condition of fixed temperature and pressure. REST2 simulation was performed as follows. Peptide atoms and side-chain atoms of MHC-class-II in contact with the peptide (henceforth, we call them the "MHC cleft") were defined as "accelerated" atoms in REST2. The MHC cleft consists of the side-chain atoms of residues 59 to 82 in the α chain and 78 to 119 in the β chain of the MHC-class-II. Interactions within the "accelerated" region, and those between the "accelerated" region and others, were then scaled according to a REST2 scheme. REST2 simulation was conducted with 24 replicas, where replica 0 corresponded to the simulation with unmodified interaction

potential, and the interaction energies within the accelerated region were halved in replica 23. Details of the REST2 simulation are described in Supporting Information. The simulation was run in NPT condition with 300 K and 1 atm. Simulations were performed using *GROMACS 2016* [49] with in-house modification to perform a Hamiltonian replica exchange method under a constant-temperature and constant-pressure (NPT) condition. The pressure was set to 1 atm. Two 200 ns REST2 simulation runs were performed for PLP136–150 and PLP139-151, respectively (9.6 μs in total). The last 100 ns runs in replica 0 were used to sample configurations. Trajectories were sampled every 20 ps.

2.13.3. Analysis of PLP structures

Cα atom coordinates of PLP, corresponding to residue IDs 140–149, were monitored and assessed with principal component analysis. For each PLP, 5000 samples from the trajectories were collected, and the combined samples (10,000 samples in total) were used to compute principal vectors [50]. The projections to the first and second principal vectors were calculated and compared. Fluctuations in all Cα atoms of the peptides were also compared. The rotation and translation during the simulation were first removed by best-fitting the MHC structures in the trajectory to the initial model. Only Cα atoms of residues 71–86 in the α chain and residues 32–216 in the β chain were considered in the fitting. The root-mean-square-fluctuations of Cα atoms in PLP were then determined for both peptide trajectories. The trajectory was split into ten 10 ns segments to analyze statistical significance (Mann–Whitney *U* test). The data were plotted and analyzed using visual molecular dynamics.

2.14. Statistical analysis

All data are presented as mean ± SEM. Mann–Whitney testing was used to analyze the EAE clinical scores, whereas cell proliferation, cytokine production, and flow cytometry data were assessed using Student's *t*-test. Statistical significance was defined as $P < 0.05$ or $P < 0.01$ using GraphPad Prism (version 8; GraphPad Software, La Jolla, CA, USA).

3. Results

3.1. Encephalitogenic peptides themselves direct the distinct clinical course of EAE

SJL/J mice were immunized with an encephalitogenic peptide (PLP136-150, PLP139-151, or PLP 178–191) to induce clinical EAE. The mice groups immunized with PLP139-151 or PLP178-191 developed RR-EAE accompanied by smoldering chronic disease, as other encephalitogenic peptides [27,31–33,51,52]. Contrastingly, those immunized with PLP136-150 developed M-EAE that quickly and fully recovered without significant residual signs (Fig. 1a). Moreover, a striking difference was observed among the groups when convalescent mice were

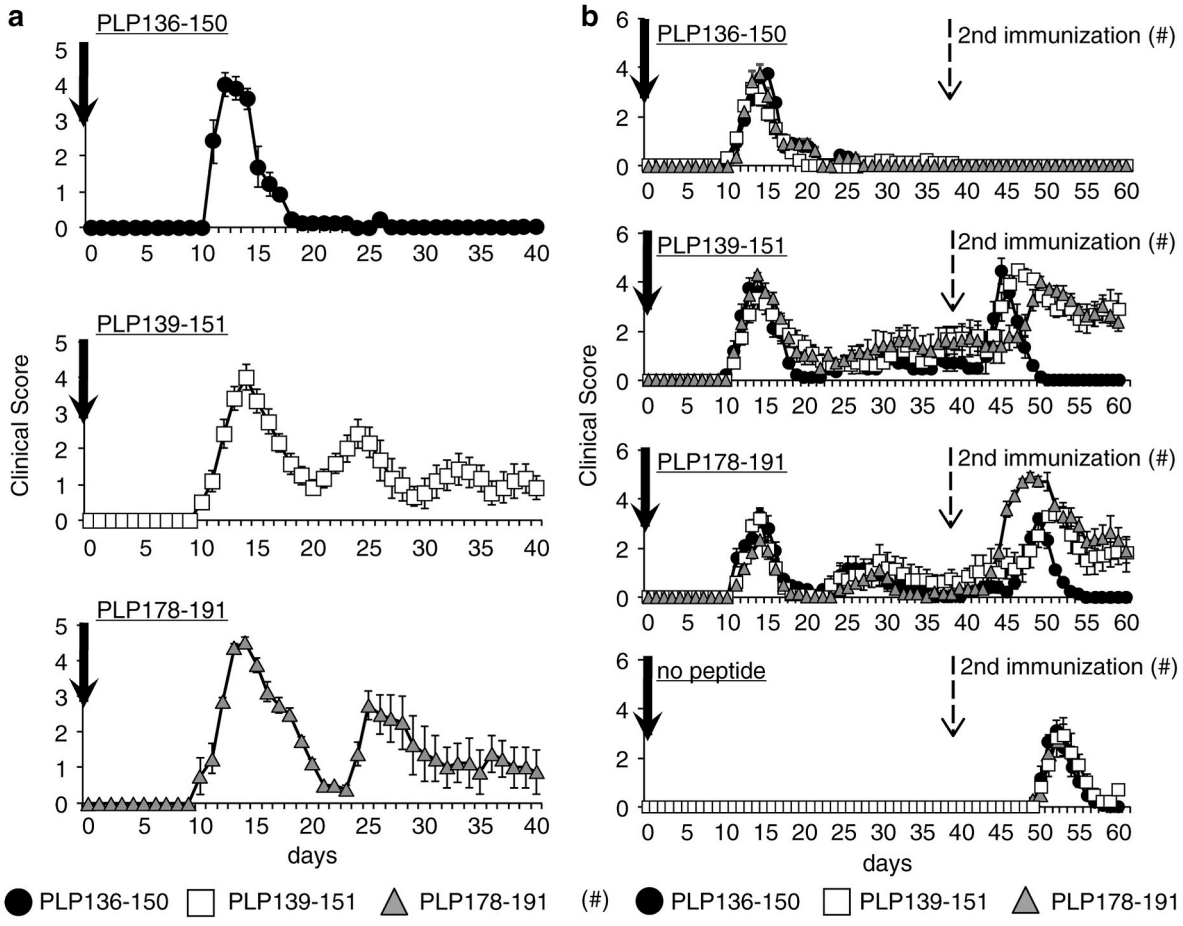

Fig. 1. Different encephalitogenic peptides direct the distinct clinical course of EAE in SJL/J mice (a) Clinical course of relapsing-remitting EAE (RR-EAE) induced with PLP139-151 or PLP178-191 versus monophasic EAE (M-EAE) induced with PLP136-150. A representative from at least seven EAE experiments is shown (n = 5 mice/group). (b) Complete resistance to EAE re-induction after recovery from PLP136-150-induced M-EAE. After recovery from primary EAE induced with the PLP-peptide, mice were re-immunized with PLP136-150, PLP139-151, or PLP178-191 on day 37. A representative from five experiments yielding similar results is shown (n = 5 mice/group). Solid and dashed arrows indicate the time of immunization and re-immunization, respectively.

re-immunized with the same, or different, peptide to induce secondary EAE. The mice first immunized with PLP139-151 or PLP178-191 developed secondary EAE, which had a more severe and progressive course, after re-immunization with any encephalitogenic peptide, except after re-immunization with PLP136-150. However, convalescent mice that received primary immunization with PLP136-150 did not develop secondary EAE with any encephalitogenic peptide (Fig. 1b). Resistance against secondary challenges for EAE differed between the EAE models.

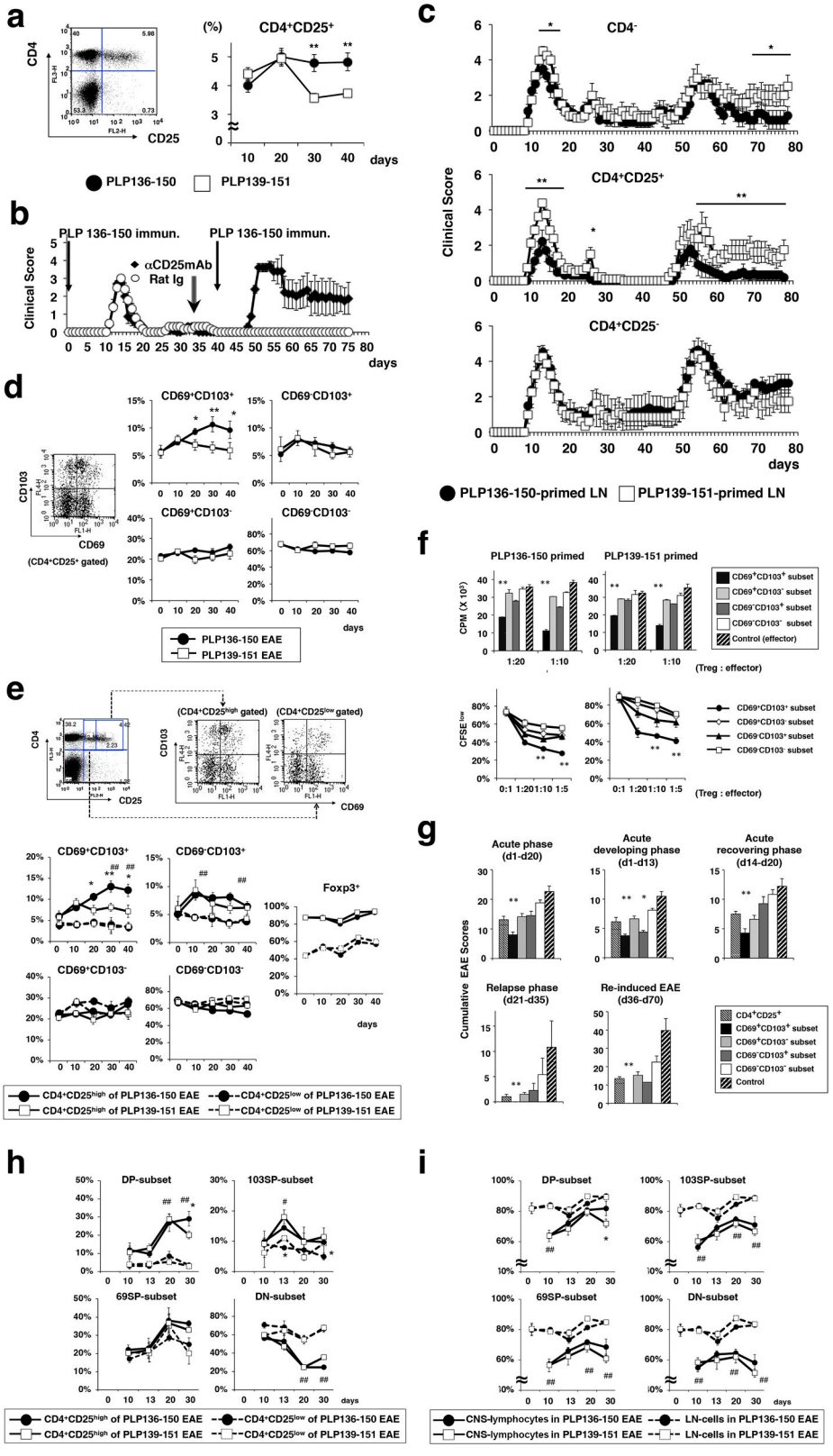

Fig. 2. Distinct quality and quantity of regulatory T-cells induced after immunization with different PLP-peptides (a) Frequency of $CD4^+CD25^+$ T-cells in PLP136-150- or PLP139-151-primed LN. Data representative of six experiments are shown (n = 6/group). (b) Abrogation of resistance to re-induction of PLP136-150-induced M-EAE after the depletion of $CD25^+$ T-cells; solid diamond: anti-CD25 mAb, open circle: rat immunoglobulin (Ig) as control. A representative from three experiments is shown (n = 5 mice/group). (c) Ability of $CD4^+CD25^+$ T-cells from PLP136-150- and PLP139-151-primed mice to suppress EAE. Data from a representative of three experiments that yielded similar results are shown (n = 5 mice/group). (d) Proportions of subpopulations demarcated by CD69 and CD103 expression among $CD4^+CD25^+$ T-cell in LNs primed with PLP136-150 or PLP139-151. Representative data from three experiments are shown (n = 6 mice/group). (e) Proportions of four subpopulations shown in (d) were compared between $CD25^{high}$ and $CD25^{low}$ fractions of $CD4^+CD25^+$ T-cells. Each fraction is indicated by a solid line and dashed line, respectively (n = 4 mice/group, $*P < 0.05$, $**P < 0.01$ between PLP136-150 priming and PLP139-151 priming: $\#P < 0.05$, $\#\#P < 0.01$ between $CD25^{high}$ and $CD25^{low}$ fractions). Foxp3 expression levels in the $CD25^{high}$ and $CD25^{low}$ fractions were also analyzed. (f) *In vitro* suppressive activity of $CD4^+CD25^+$ T-cell subpopulations isolated on d30 from pooled LN cells primed with either PLP-peptides and mixed with PLP139-151-primed effector cells under PLP139-151 stimulation on cell proliferation rates using recall response assay (upper panel) or CFSE-labeling assay (lower panel). Assays were conducted in at least 4 wells, and data are expressed as the mean ± SEM. ($**P < 0.01$ compared with control, CPM: count/min). (g) *In vivo* suppressive activity of the $CD4^+CD25^+$ T-cell subpopulations. Clinical scores during the acute phase of EAE (d1-d20) and relapse phase (d21-d35) were recorded and summated daily (n = 5 mice/group, $*P < 0.05$, $**P < 0.01$). The acute phase was separated into the acute developing (d1-d13) and acute recovering (d14-20) phases. The same mice were re-immunized with PLP139-151 on d35, and clinical scores of the re-induction phase were recorded daily from d36 to d70. (h, i) Kinetics and phenotype changes of CNS-infiltrating cells in mice primed with PLP136-150 and PLP139-151. CNS-infiltrating lymphocytes were collected using a Percoll gradient, enumerated, and examined for markers of $CD4^+CD25^+$ T-cells through flow cytometry and compared with those in LN cells (n = 4 mice/group, $*P < 0.05$; $**P < 0.01$ between PLP136-150 and PLP139-151 priming, $\#P < 0.05$; $\#\#P < 0.01$ between CNS and LN cells). (h) Frequencies of the $CD4^+CD25^+$ T-cell subpopulations in CNS cells between $CD25^{high}$ and $CD25^{low}$ components indicated by the solid line and dashed line, respectively. (i) Foxp3 expression in the $CD4^+CD25^+$ T-cell subpopulations in CNS lymphocytes (solid line), when compared with those in LN cells (dashed line), $*P < 0.05$, $**P < 0.01$.

3.2. Different PLP-peptides induce distinct regulatory T-cells in quality and quantity

PLP136-150 was suspected of inducing antigen-nonspecific resistance to autoimmune diseases. This was supported by the observation that, during the convalescence of PLP136-150-EAE, mice were partially protected from CIA via challenge with type II collagen when compared with that of PLP139-151-EAE (Supplementary Fig. S1). However, the preventive effects of PLP136-150 for CIA were much weaker than for EAE, indicating that the antigen-nonspecific effects of PLP136-150 were inferior to the antigen or disease targets' preferential effects.

We then evaluated the possible differences in priming ability for each peptide to elicit encephalitogenic T-cells. Regardless of immunization with PLP136-150 or PLP139-151, the primed LN cells showed similar proliferative responses and production of proinflammatory cytokines interferon-γ (IFN- γ) and interleukin (IL)-17 on day 10 (d10); additionally, the recall responses substantially decreased on d20 in parallel with recovery from primary EAE. However, on d30 and d40, PLP136-150-primed LN cells continued to display reduced recall responses, whereas PLP139-151-primed LN cells restored responses (Supplementary Fig. S2a). Of interest, *in vitro* stimulation with the same peptide induced higher responses than stimulation with other peptide, regardless of the priming peptide. The timing of the restored responses was consistent with that of the relapses in the PLP139-151-immunized mice. Hence, the persistently lower recall responses of the PLP136-150-primed LN cells from d20–d40 might have resulted from the induction of regulatory cells in the LNs. Consistently, the transfer of PLP136-150-primed LN cells from d30 and d40 mice weakly but significantly suppressed primary EAE attack and subsequent relapses induced in the recipient mice, compared with the transfer of PLP139-151-primed LN cells (Supplementary Fig. S2b).

We then sought to determine whether $CD4^+CD25^+$ Tregs [53] are differentially involved in PLP136-150- and PLP139-151-EAE. The frequency of $CD4^+CD25^+$ T-cells in the LN increased on d20 in both EAEs and was maintained in the PLP136-150-immunized mice but was reduced in the PLP139-151-immunized mice on d30 and d40 (Fig. 2a), which was paralleled with peptide-specific T-cell recall responses (Supplementary Fig. S2a).

We next injected anti-CD25 mAb into mice during the convalescent phase of M-EAE on d35, which fully recovered the susceptibility of mice to secondary EAE, the signs of which were serious and persistent (Fig. 2b). Upon transfer, purified $CD4^+CD25^+$ T-cells from PLP136-150-primed LN cells exhibited a more potent regulatory activity than those from the PLP139-151-primed LN cells (Fig. 2c). Collectively, we concluded that $CD4^+CD25^+$ T-cells induced in PLP136-150-primed mice contributed to the acquisition of resistance to disease reactivation, i.e., spontaneous relapse and induction of secondary EAE.

3.3. Induction and maintenance of $CD69^+CD103^+$ regulatory T-cells in M-EAE

We subsequently quantified the expression of the key Treg factor Foxp3 [54] in $CD4^+CD25^+$ T-cells derived from LN cells during M-EAE and RR-EAE and observed no significant difference between them (Supplementary Figs. S2c and d). $Foxp3^+CD4^+CD25^+$ Tregs express various surface markers [55], among which integrin $\alpha_E\beta_7$ (CD103) is a marker of recently activated cells and identifies one of the most potent regulatory cell types in mice [56,57]. We measured the expression of CD103 and another activation marker, CD69 [57,58], both of which are associated with transforming growth factor (TGF)-β expression [59,60], in LN $CD4^+CD25^+$ T-cells. The frequency of the $CD69^+CD103^+$ subpopulation of $CD4^+CD25^+$ T-cells was higher in M-EAE than in RR-EAE from d20-d40, whereas the $CD69^+CD103^-$ and $CD69^-CD103^+$ subpopulations of the $CD4^+CD25^+$ T-cells were similar in both EAE models (Fig. 2d). The differences in the frequencies of the $CD69^+CD103^+$ subpopulation between the EAE models were observed exclusively in the $CD25^{high}$ fraction of $CD4^+CD25^+$ T-cells, wherein Foxp3 expression was homogeneously bright (Fig. 2e). The $CD69^+CD103^+$ subpopulation isolated from d30 LN cells showed a more potent suppression capacity than other subpopulations *in vitro* and *in vivo*, regardless of the priming peptide (Fig. 2f and g). In contrast, the $CD69^+CD103^-$ and $CD69^-CD103^+$ subpopulations showed only mild suppression shortly after, and before, the EAE attack peak, respectively (Fig. 2g). These results indicated that the $CD69^+CD103^+$ subpopulation represented the most efficacious Tregs, and the selective expansion of this subpopulation may account for the continuous resistance to re-induction and prevention of EAE relapse in PLP136-150-primed mice. We operationally referred to the $CD69^+CD103^+$, $CD69^+CD103^-$, $CD69^-CD103^+$, and $CD69^-CD103^-$ subpopulations as DP, 69SP, 103SP, and DN subsets, respectively.

Tregs presented in the CNS during the acute phase of EAE are thought to resolve local inflammation [61]. Although the generation of Tregs *in situ* from infiltrated effector cells by contact with neurons has been reported in the resolution [62], another study showed that infiltrated Tregs may lose Foxp3 expression and suppressive potentials in the CNS inflammatory milieu [63]. We further analyzed the characteristics of the Treg subsets among lymphocytes in the CNS of M-EAE and RR-EAE mice. The DP subset of the $CD25^{high}$ fraction expanded in the CNS after both EAE peaks (d20), which was more remarkable than the expansion observed in the draining LN (Fig. 2h). The most active DP subset was maintained on d30 in M-EAE compared with RR-EAE. Contrastingly, the 103SP subset, save for its $CD25^{low}$ fraction in M-EAE, infiltrated the CNS only during the disease peak (d13), and its $CD25^{low}$ fraction in RR-EAE re-infiltrated the CNS at relapse (d30) (Fig. 2h). Furthermore, Treg subsets in the CNS contained lower proportions of $Foxp3^+$ cells than those in the LN (Fig. 2i), indicating a possible loss of Foxp3 expression in the CNS. However, only the DP subset preserved $Foxp3^+$ cells relatively well in the CNS, particularly after the disease peak (Fig. 2i). Given that DP subsets of $CD4^+CD25^+$ T-cells maintained Foxp3 expression in the inflammatory CNS lesions, we postulated that they might efficiently inhibit the reactivation of pathogenic effector cells in the CNS.

3.4. Hierarchy and cross-reactivity of encephalitogenic peptides in SJL/J mice

Our results indicate that PLP136-150 more efficiently induces a DP subset of Treg; hence, PLP136-150 EAE is monophasic and resistant against the re-induction of secondary EAE. The differential abilities of the overlapping peptides were further analyzed using *in vivo* and *ex vivo* experiments. Earlier studies emphasized that PLP139-151 is an immunodominant peptide in SJL/J mice, as whole CNS tissue-primed cells readily respond to this peptide [64]. Similarly, we immunized SJL/J mice with spinal cord homogenates (SCH) and examined the T-cell recall response to peptides encephalitogenic for SJL/J mice. Both PLP136-150 and PLP139-151 were deemed dominant peptides, as the SCH-primed LN cells responded to these peptides (Fig. 3a). Accordingly, PLP178-191, MBP89-101, and MOG92-106 were thought to be cryptic (Fig. 3a). Interestingly, the T-cells primed with a dominant peptide did not react to cryptic peptides, whereas T-cells primed with a cryptic peptide showed weak, but apparent reactivity to dominant peptides (Fig. 3b). This cross-response to dominant peptides, particularly PLP136-150, was also observed to some extent with peptide-free CFA immunization (Fig. 3b). These results indicated that autoimmune T-cells reactive to the dominant PLP-peptides might represent an intrinsic component of the immune system, although immunization with an encephalitogenic peptide is needed for EAE development.

Of interest, once SJL/J mice were primed with dominant PLP-peptides, the preferential reactivity to these peptides was preserved even after secondary immunization with other encephalitogenic peptides (Fig. 4 upper). In contrast, when mice were primed with cryptic peptides, immune responses to these peptides appeared to be

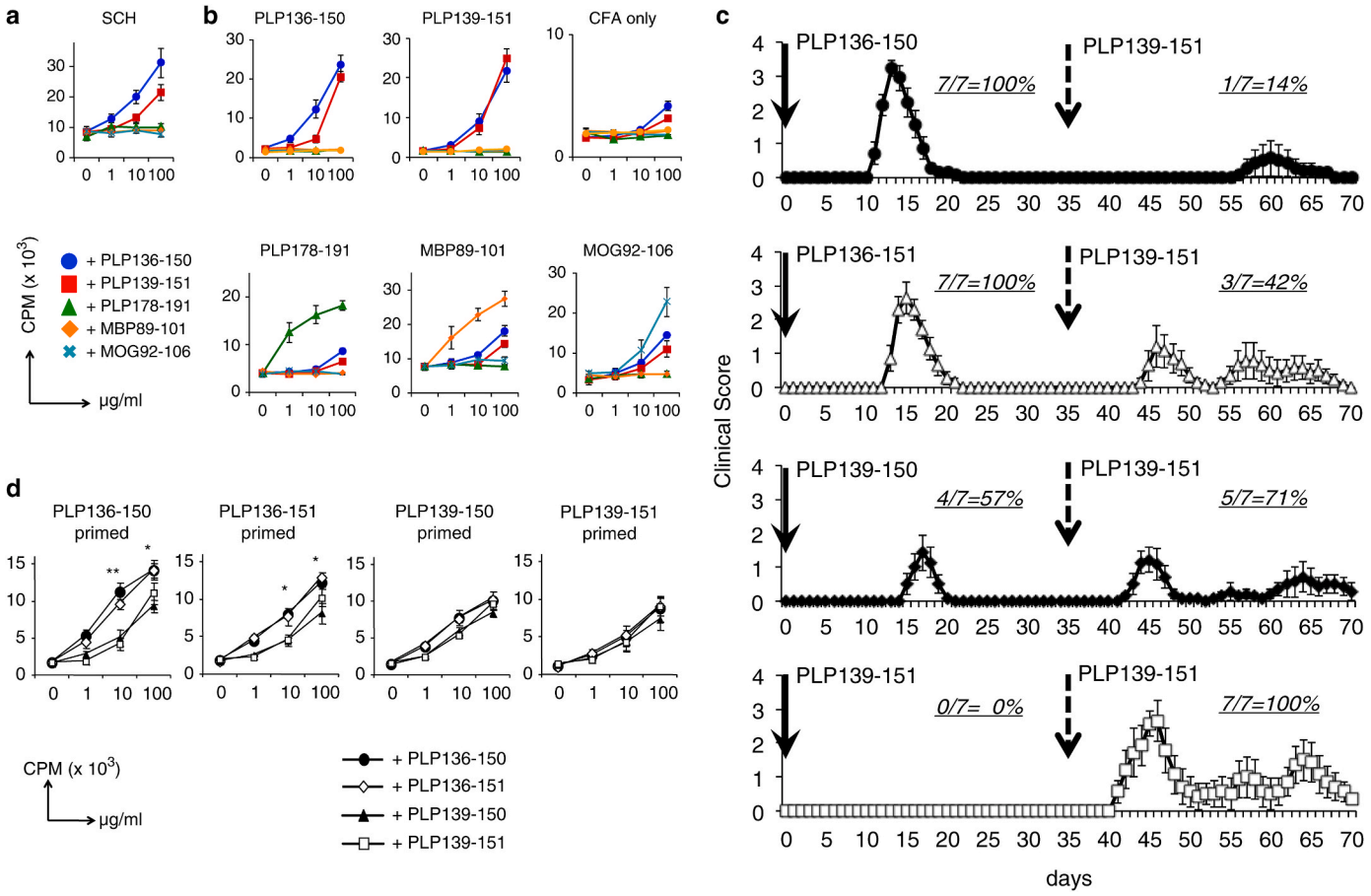

Fig. 3. Hierarchy and cross-reactivity of encephalitogenic peptides in SJL/J mice (a) Recall response of the LN cells from naïve SJL/J mice primed with spinal cord homogenate. Proliferative responses to encephalitogenic peptides PLP136-150, PLP139-151, PLP178-191, MBP89-101 and MOG92-106 were measured on d13 after immunization. Representative data from one of two experiments with similar results (n = 4 mice/group, CPM: count/min) are shown. (b) Recall responses of the primed LN cells to encephalitogenic peptides. SJL/J mice were primed with each encephalitogenic peptide in CFA or with CFA without the peptide as a control, and proliferative responses were measured on d13. Representative data from one of at least three experiments with similar results (n = 5 mice/group, CPM: count/min) are shown. (c) Primary EAE was induced with a low-dose (10 µg/mice) of overlapping PLP-peptide (PLP136-150, PLP136-151, PLP139-150, or PLP139-151) as a suboptimal stimulus, and secondary EAE was induced with a regular dose (100 µg/mice) of PLP139-151. The clinical scores for the mice that developed clinical signs of EAE, and the incidence of EAE among immunized mice, are shown (n = 7 mice/group, $^{*}P < 0.05$, $^{**}P < 0.01$). Arrows indicate the time of immunization. (d) Recall response to four overlapping PLP-peptides (PLP136-150, PLP136-151, PLP139-150, or PLP139-151). Proliferative responses of LN cells primed with suboptimal doses of peptide were measured on d13. Representative data from one of two experiments with similar results are shown (n = 4 mice/group, CPM: count/min).

subdominant after secondary immunization with other encephalitogenic peptides (Fig. 4 lower). Hence, T-cell reactivity to a dominant PLP-peptide overwhelmed other encephalitogenic T-cell responses in SJL/J mice. Particularly, it appears that PLP136-150- and PLP139-151-reactive T-cells did not completely overlap, as PLP136-150-primed LN cells responded more robustly to PLP136-150 than to PLP139-151 at low concentrations, whereas PLP139-151-primed LN cells responded relatively equally to both dominant peptides (Fig. 3b).

We then evaluated whether T-cell responses to a dominant PLP-peptide were preserved after inducing tolerance with another dominant PLP-peptide. PLP136-150 induced comparably complete tolerance to PLP136-150 and PLP139-151, whereas PLP139-151 induced sufficient tolerance only to PLP139-151, but partial tolerance to PLP136-150 (Supplementary Fig. S3a). In addition, mixtures of both dominant peptides induced M-EAE, similar to PLP136-150-EAE; LN cells primed with the peptide mixture exhibited lower proliferative responses to the peptide, similar to PLP136-150-primed LN cells (Supplementary Figs. S3b and c). We hypothesized that they have different functional avidity.

Biological phenomena resulting from the differential avidity between the T-cell receptor (TCR) and peptide/MHC complex can be overlooked when a supra-optimal peptide dose is applied [65]. Therefore, we re-evaluated the encephalitogenic capacity of PLP-peptides using a lower immunizing dose (10 µg/mouse, 1:10 of the optimal dose). At this suboptimal dose, sensitization to PLP139-151 did not induce EAE at all, strongly supporting the qualitative differences between PLP136-150 and PLP139-151 and rejecting the hypothesis that both peptides can be grouped based on their ability to stimulate SCH-primed LN cells. We also conducted a more comprehensive analysis by adding two overlapping peptides, PLP136-151 and PLP139-150. The results revealed a hierarchy among these peptides regarding encephalitogenic potential to induce primary EAE (PLP136-150 > PLP136-151 > PLP139-150 > PLP139-151) (Fig. 3c). In parallel, we evaluated the recall responses to the PLP-peptides in mice primed with a suboptimal dose. LN T-cells primed with a less encephalitogenic peptide, such as PLP139-151, responded equally to any peptide with a higher encephalitogenic potential, whereas T-cells primed with a more encephalitogenic peptide responded more efficiently to peptides with higher encephalitogenicity, indicating that priming with a more encephalitogenic peptide could result in a repertoire skewed to the primed peptide itself (Fig. 3d). Conversely, susceptibility to EAE re-induction with secondary immunization was inversely correlated with the encephalitogenic potential of peptides used for primary immunization (Fig. 3c). These results indicated that such preferential skewing of T-cells to the peptide placed at a higher rank in the

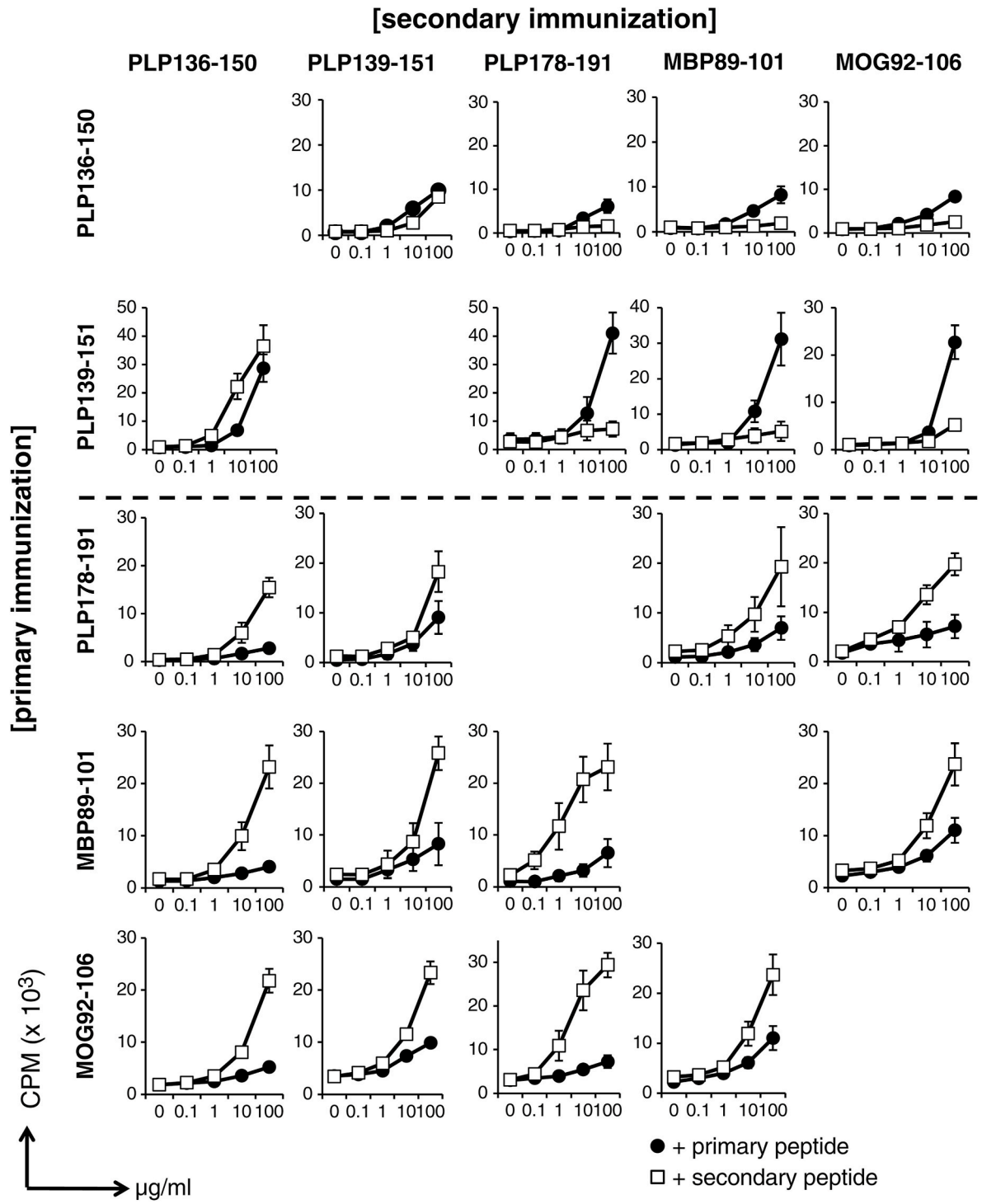

Fig. 4. Longitudinal reactivity in sequential immunization Mice sensitized with an encephalitogenic peptide (primary peptide; PLP136-150, PLP139-151, PLP178-191, MBP89-101, or MOG92-106) were immunized with another peptide (secondary peptide; PLP136-150, PLP139-151, PLP178-191, MBP89-101, or MOG92-106) on d40, and the recall proliferative responses to both peptides in the LN cells of the mice was measured on d13 after secondary immunization. Representative data from one of two experiments with similar results are shown (n = 5 mice per group, CPM: count/min).

encephalitogenic hierarchy could be critical for inducing primary EAE, as well as resistance to disease re-induction and reactivation of encephalitogenic T-cells.

3.5. Distinct antigen specificity of Treg subsets in PLP136-150 and PLP139-151-induced EAEs

Collective data suggests that the preferential reactivity of the peptide-primed T-cells to the dominant PLP-peptide may reflect the abundance of T-cells reactive to the dominant peptide. Using PLP139-151-bound I–As MHC-class II dextramer [38,39], we compared the frequency of the cells reactive to the dominant peptide among total $CD4^+$ T-cells, $CD4^+CD25^+$ T-cells ($CD25^+$), and $CD4^+CD25^-$ T-cells ($CD25^-$) between PLP136-150- and PLP139-151-primed LN cells (Fig. 5a). Although $dextramer^+$ populations were primarily detected in $CD25^-$ cells during the induction phase of EAE (d10 and d13), these populations

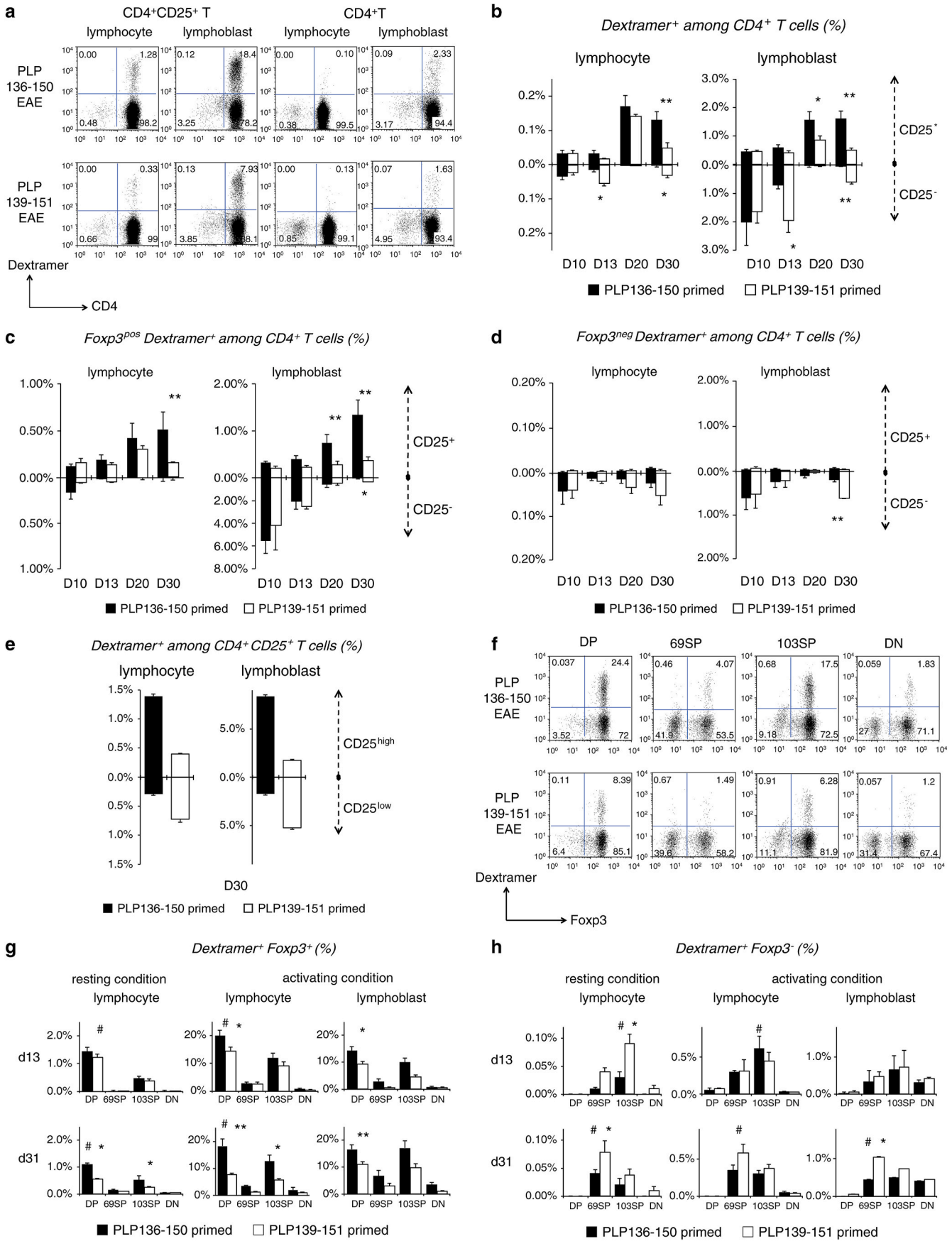

(caption on next page)

Fig. 5. Distinct antigen specificity of Tregs subsets in PLP136-150 and PLP139-151-induced EAEs (a, b) Frequency of PLP139-151-specific I–As dextramer$^+$ cells in isolated CD4$^+$ T-cells and CD4$^+$CD25$^+$ T-cells. (a) Representative staining pattern on d30. (b) Frequency of dextramer$^+$ cells in lymphocyte and lymphoblast fractions. Populations with Forward Scatter (FSCs) larger than their lymphocytes were demarcated as lymphoblast. (c, d) Frequency of Fox3$^+$ dextramer$^+$ cells or Fox3$^-$ dextramer$^+$ cells in isolated CD4$^+$CD25$^+$ T-cells and CD4$^+$CD25$^-$ T-cells, represented as the percentage among CD4$^+$ T-cells. (e) Frequency of dextramer$^+$ cells in CD25^{high} and CD25^{low} fractions among CD4$^+$CD25$^+$ T-cells on d30. (f–h) Frequency of dextramer$^+$ cells in the subset of CD4$^+$CD25$^+$ T-cells. (f) Representative staining pattern on d30. (g, h) Frequency of dextramer$^+$ cells in Foxp3$^+$ and Foxp3$^-$ fractions on d13 and d30. Representative data from one of the two experiments are shown (*$P < 0.05$, **$P < 0.01$ between PLP136-150 and PLP139-151 priming; #$P < 0.05$, ##$P < 0.01$ among the subsets of Treg).

mostly shifted in CD25$^+$ cells during the recovery phase (d20) for both groups (Fig. 5b). Although dextramer$^+$ populations in PLP136-150-primed LN cells continuously resided exclusively in CD25$^+$ cells during the remission phase (d30), approximately half of these populations were found in CD25$^-$ populations in PLP139-151-primed LN cells (Fig. 5b). Foxp3$^+$dextramer$^+$ populations were mostly CD25$^-$ during the induction phase (d10 and d13), indicating activation-induced expression of Foxp3 [66]. In contrast, during the recovery and remission phases of EAE (d20 and d30), Foxp3 expression was largely restricted to CD25$^+$ cells in PLP136-150-primed LN cells (Fig. 5c and d). The same trend was observed in PLP139-151-primed LN cells, though it was less remarkable. These results indicated that the Foxp3$^+$dextramer$^+$ cells detected during the remission phase were intrinsic Tregs.

Moreover, dextramer$^+$CD4$^+$CD25$^+$ T-cells were primarily detected in the CD25^{high} fraction during the remission phase (d30) of PLP136-150-EAE, whereas they were observed mostly in the CD25^{low} fraction after PLP139-151 priming (Fig. 5e). Furthermore, among the Treg subsets defined by the expression of CD103 and CD69, most of the dextramer$^+$Foxp3$^+$ populations were observed in the DP and 103SP subsets regardless of immunization with PLP136-150 or PLP139-151 (Fig. 5f). When these subsets were compared on d13 and d31, the proportion of dextramer$^+$Foxp3$^+$ populations was higher in the DP than 103SP subsets in both the PLP136-150- and PLP139-151-primed groups. Although the high proportion of dextramer$^+$Foxp3$^+$ populations in the DP subset was maintained in the PLP136-150-primed LN cells, it decreased in PLP139-151-primed LN cells (Fig. 5g). In contrast, dextramer$^+$Foxp3$^-$ cells were relatively undetectable in the DP subset but were present in the 103SP subset on d13 and the 69SP subset on d31,

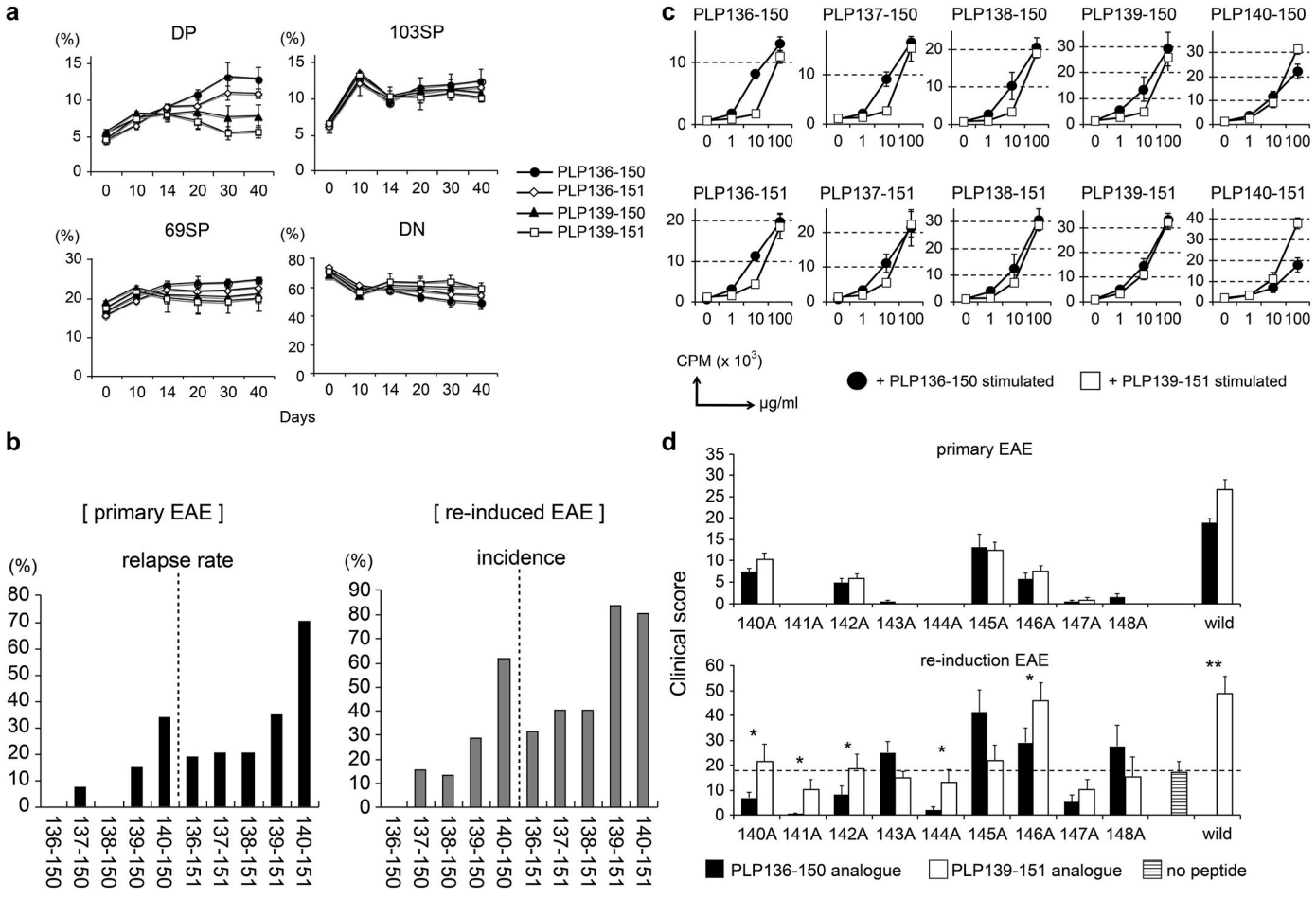

Fig. 6. Resistance to the re-induction of EAE via expansion of a distinct subset of Tregs depends on the flanking residues of the dominant peptides that are reflected in the peptide preferences. (a) Different kinetics of CD4$^+$CD25$^+$ T-cell subsets in LN cells primed with overlapping PLP-peptides (PLP136-150, PLP136-151, PLP139-150, or PLP139-151). LN cells from an individual mouse were individually analyzed (n = 5 mice/group). (b) Comparison of overlapping PLP-peptides (PLP13x-15 y (x = 6–9; y = 0,1)). The relapse rate (%) of primary EAE and the incidence (%) of re-induced EAE are shown (n = 10–28 for each group). (c) Recall response to PLP136-150 and PLP139-151 on d40 in LN cells of SJL/J mice primed with each truncated PLP-peptide indicated in Fig. 6b. (n = 4 mice/group). Note that the scale of CPM differs (CPM: count/min). (d) Differences in susceptibility to EAE induced with the PLP-peptides depend on the PLP136-150 or PLP139-151 backbone (n = 5 mice/group).

particularly after PLP139-151 priming (Fig. 5h). Thus, the dextramer^{+} DP subset was exclusively Foxp3^{+} Tregs, whereas the dextramer^{+} 103SP subset also contained a Foxp3^{-} non-Treg fraction. These results implied that PLP136-150 priming could efficiently induce and maintain antigen-specific Foxp3^{+} Tregs; however, antigen-specific non-Tregs were excluded. Additionally, PLP139-151 priming induced antigen-specific Foxp3^{+} Tregs, which were only transient and rapidly replaced by antigen-specific non-Tregs.

3.6. PLP136-150 residues determine the dominant peptides hierarchy and reactivation resistance

We then compared the frequency of the Treg subsets shown in Fig. 2d isolated from the LN cells primed with overlapping peptides PLP136-150, PLP136-151, PLP139-150, and PLP139-151, which expressed different levels of encephalitogenicity shown in Fig. 3c. The DP subset increased continuously in mice primed with the more dominant PLP-peptides 136–150 and 136–151, while they decreased when mice were immunized with less dominant peptides. Other subsets, such as 69SP, 103SP, and DN, were similar across all groups of mice (Fig. 6a). The kinetics in the DP subset appeared to correlate with the ability of each primed peptide to induce primary EAE and to protect against secondary EAE.

The linkage between the functional and structural aspects of PLP-peptide priming was then assessed. The TCR contact residues and MHC binding sites are thought to be identical between PLP136-150 and PLP139-151 as the T-cells primed with both PLP-peptides were highly cross-reactive (Fig. 3b). Thus, the presence of N-terminal residues (R136/V137/S138) and/or absence of C-terminal residue (F151) likely accounted for different encephalitogenicity and protection against secondary EAE, coupled with the ability to induce the DP subset of Tregs.

To further confirm this, we immunized mice with a larger panel of overlapping PLP-peptides at regular optimal doses and analyzed the clinical manifestations of the primary and secondary EAE and the T-cell recall response during the remission phase of primary EAE. Deletion of 1–4 residues in the N-terminus (R136, V137, S138, and H139) from PLP136-150 and the addition of one residue (F151) to the C-terminus synergistically increased the relapse rate of primary EAE and the incidence of secondary EAE (Fig. 6b). The recall response was also enhanced in correlation with the EAE clinical courses (Fig. 6c). We then compared the clinical profile of the EAE in mice immunized with analog peptides of PLP136-150 and PLP139-151 with amino acid substitutions. The analog peptides had substitutions at S/C140, L141, G142, K143, W144, L145, G146, H147, or P148 to A (alanine). Immunization with any of the peptide analogs proved less efficient for the induction of primary EAE, especially L141A, K143A, W144A, H147A, and P148A, when compared with the wild peptide; regardless of whether the analog was derived from PLP136-150 or PLP139-151 (Fig. 6d upper). In contrast to the wild PLP136-150 peptide, mice primed with the PLP136-150 analog peptides developed secondary EAE, although disease severity was reduced compared with those primed with the PLP139-151 analog, save for the K143A, L145A, and P148A analog peptides. Like the priming with wild PLP139-151, priming with the PLP139-151 analog peptides also resulted in secondary EAE, although some exerted marginal preventive effects were comparable to priming without a peptide (Fig. 6d lower).

Furthermore, the T-cell recall response in the LNs of mice immunized with analog peptides showed that immunization with the K143A and P148A substituted peptides did not induce T-cell responses to any peptide, whereas immunization with the W144A, H147A, and L141A substituted peptides induced T-cell responses only to the analog peptide itself (Fig. 7a). Together with the results that these analog peptides did not induce primary EAE (Fig. 6d upper), these results indicate that K143 and P148 may serve as MHC binding sites, while W144, H147, and L141 could be TCR contact sites in both PLP-peptides [67]. The I–As binding residues of the PLP-peptides, which we assumed in this study, were consistent with those previously proposed as I–As ligand motifs [68]. A previous study demonstrated that while using T-cell clones specific for PLP139–151, W144, H147, and L141 function as the primary, secondary, and tertiary TCR contact sites, respectively, whereas P148 (P9) and K143 (P4) or L145 (P6) are the primary and secondary MHC binding sites, respectively [67–70]. Taken together, we regarded R136-S138 of PLP136–150 and F151 of PLP139-151 as the flanking residues, which were located outside the TCR contact sites and MHC binding sites. These results indicated that MHC-class II binding and TCR contact residues were shared between PLP136-150 and PLP139-151 and that flanking residues played a critical role in determining the hierarchy in encephalitogenic potentials and the induction of the DP subset of Tregs, which plays a pivotal role in the regulation of the EAE clinical course.

3.7. PLP136-150 flanking residues secure binding stability to the MHC-class II molecules

According to the analysis of the T-cell response with analog peptides (Fig. 7a), S140 and L145 in PLP136-150 were speculated to be secondary MHC binding sites, corresponding to P1 and P6 that were defined by the ligand motifs [68]. In addition, the presence of another binding pattern to I–As, shifted toward the N-terminal side by three residues, such as K143 corresponding to P1 instead of P4, and P148 corresponding to P6 instead of P9, could not be excluded for PLP139-151 (Fig. 7b). These results prompted us to explore if PLP136-150 and PLP139-151 binding to I–As differs qualitatively or quantitatively. The binding capacity of the dominant PLP-peptides to MHC molecules was therefore evaluated *in silico*. We first composed estimated I–As α and β chains, MHC-class II of SJL/J mice, and the two PLP-peptides by homology modeling (Fig. 8a, Supplementary Fig. S4). We then simulated their structural changes in solution using calculations of their molecular dynamics (MD) and replica exchange with solute tempering (REST) [48]. This simulation revealed that PLP136-150 remained stationary in the MHC groove, while PLP139-151 escaped the groove and fluctuated around it, and that the N-terminal residues of these PLP-peptides were located outside of the MHC groove, which supports the notion that these residues correspond to flanking residues (Video 1). Focusing on the main chain of the common core peptides 140–149, PLP136-150 was quite stabilized at a single center in association with its N-terminal residues, whereas PLP139-151 was unstable with nearly double the foci (Fig. 8b and c). This stability of PLP136-150 relied on the presence of high hydrogen bond occupancy at L145, H139, S138, and K150 of its main chain with MHC molecules (Table 1), the presence of the side-chains at L141 and W144 that could fit in the mostly hydrophobic pockets of the MHC molecules (Supplementary Figs. S5a and b), and the presence of weak hydrogen bonds at K143 and S138 of its side-chain (Supplementary Figs. S5c and d). The presence of synergistic hydrogen bonds at residues R136-S138 of PLP136-150 (Fig. 8d) and the absence of the residue F151 of PLP139-151, which obstructed the formation of strong hydrogen bonds at K150 made by a turn shaped from P148 (Fig. 8e), could achieve these phenomena. In contrast, PLP139-151 formed no stable hydrogen bonds from H147 to K150 of its main chain with the MHC molecules (Table 1), consistent with the observations that the C-termini of PLP139−151 displayed a variety of conformations (Fig. 6a, Video 1). Furthermore, even the hydrogen bonds formed at the N-terminal residues of the main chain were weak (Table 1), and the overall contact of its side-chain with MHC molecules was less than that of PLP136-150, especially at W144 and H147 in the hydrophobic pockets (Supplementary Fig. S5e), suggesting an inability to stabilize in the shifted position to the N-terminal side. These results indicated that PLP136-150 could strictly bind to the MHC molecules, while PLP139-151 would loosely bind and move back and forth. Taken together, the binding stability of the PLP-peptides to MHC molecules was structurally influenced by their flanking residues, which determined the encephalitogenic potential and stability of antigen-specific Tregs (Fig. 8f).

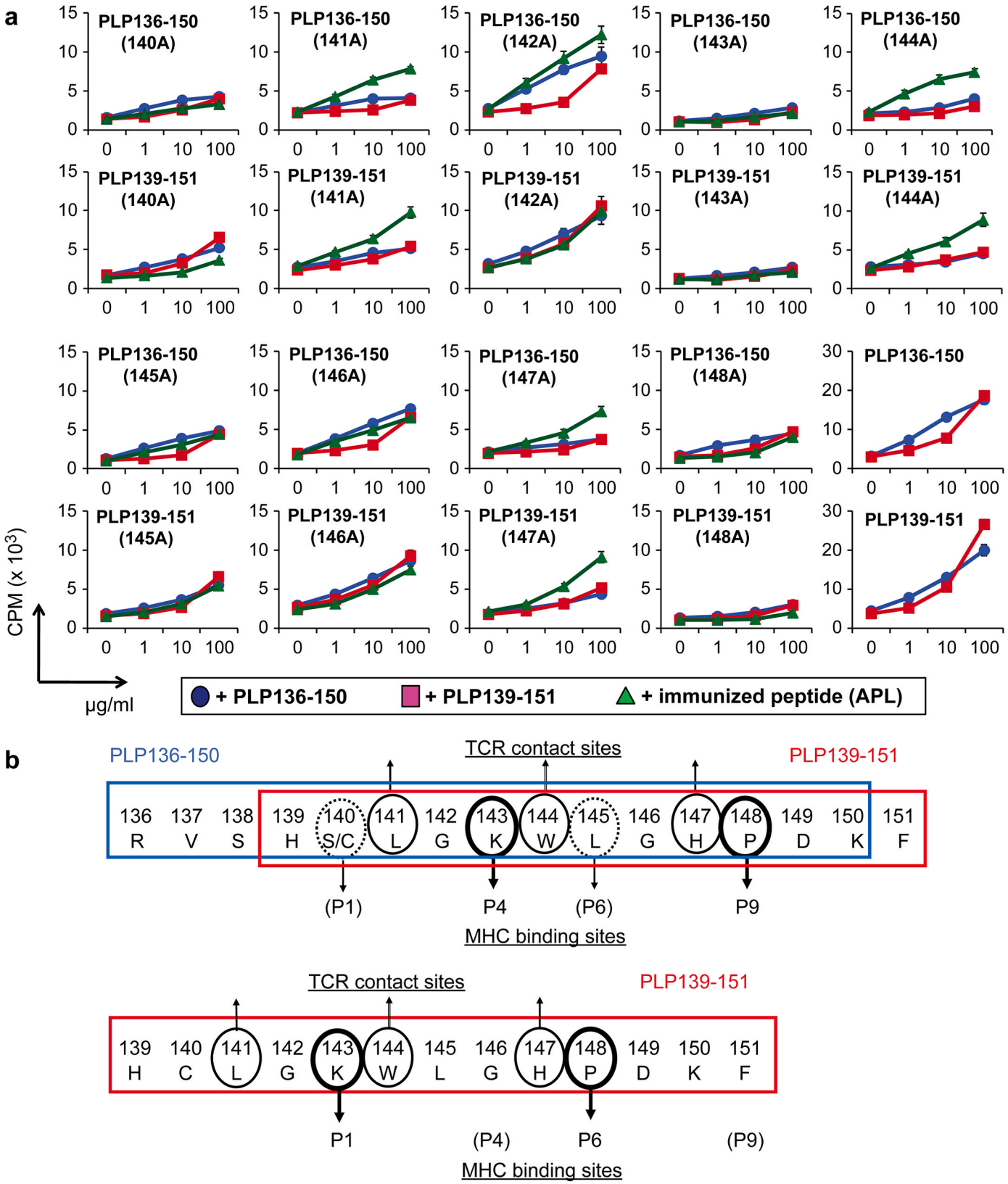

Fig. 7. MHC binding sites and TCR contact sites of PLP136-150 and PLP139-151 (a) Estimation of MHC binding sites and TCR contact sites of PLP-peptides. Altered peptides derived from PLP136-150 or PLP139-151 was prepared by substituting each residue from C/S140 to P148 with alanine (A). Mice were primed with the altered peptide ligand (APL), and recall responses to APL, PLP136-150 and PLP139-151 of primed LN cells were compared. Representative data from one of two experiments with similar results are shown (n = 3 mice/group, CPM: count/min). (b) Topology of PLP-peptide sequences and estimated role of each residue as expected from Figs. 6d and 7a. The key residues are encircled with ovals. P1, P4, P6, and P9 are thought to correspond to MHC pockets as described in the binding motif.

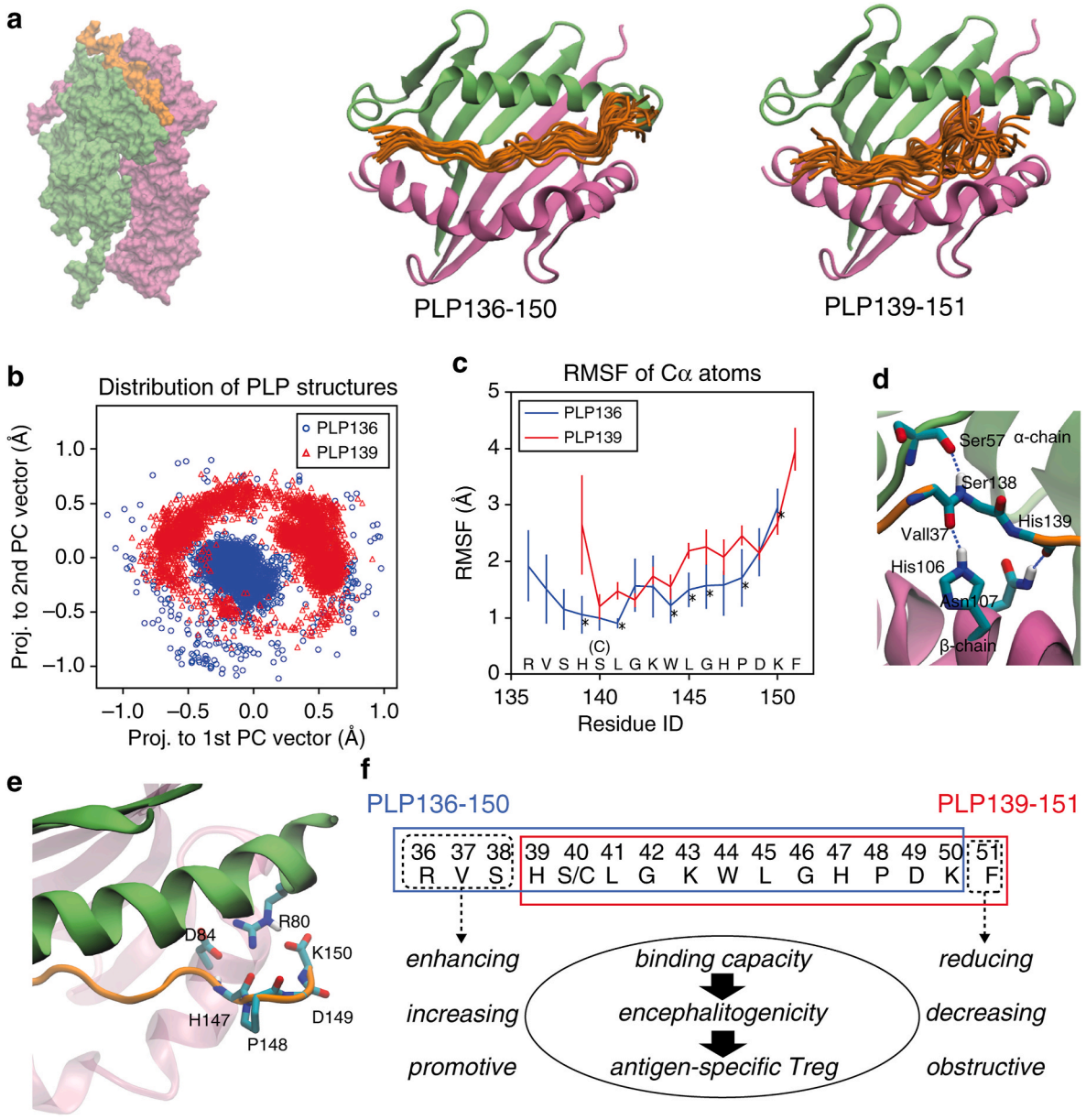

Fig. 8. Binding stability of PLP-peptides to MHC-class II molecules *in silico* (a) Overall structure of MHC-class II I–As α and β chains and PLP (left panel). Green: MHC-class II α chain, Purple: MHC-class II β chains, Orange: PLP. Structures of the PLP136–150 and PLP139–151 peptide main chains observed during a simulation (middle and right panel, respectively). PLP structures were sampled at 5 ns intervals and 20 structures are indicated, whereas MHC was fixed at the initial configuration. (b) Distribution of PLP structures projected to the top two principal vectors. Projections to the first and the second principal vectors were calculated based on the trajectories of the PLP Cα atom coordinates. (c) Root-mean-square-fluctuation of PLP Cα atoms. Asterisks indicate significantly smaller or larger fluctuations when compared with those of the other chain (Mann-Whitney test). (d) Key hydrogen bonds between N-terminal residues of PLP136–150 and MHC-class II molecules. A snapshot of the interaction at 150 ns of the simulation was depicted (left panel). Distribution of the atom-atom distances between three donor-acceptor pairs of the hydrogen bonds (right panel). (e) Key hydrogen bonds between C-terminal residues of PLP136–150 and MHC-class II molecules. A snapshot of the interaction at 150 ns of the simulation was depicted. (f) Topology of PLP-peptide sequences and estimated role of flanking residues.

3.8. EAE reactivation resistance in PLP136-150 priming requires peptide immunization itself

To examine the potential therapeutic applications of the results for autoimmune diseases, we evaluated whether the resistance to EAE reactivation observed in PLP136-150 priming could be induced without primary EAE development. Classical tolerance induction with peptides administrated orally or intravenously inhibited the development of EAE [71,72]. We found that this peptide-induced tolerance was observed only in a peptide-specific manner (Fig. 9a), except for cross-tolerance between PLP136-150 and PLP139-151. In contrast, subcutaneous sensitization with the peptide emulsified in incomplete Freund's adjuvant instead of CFA (peptide/IFA sc) did not induce primary EAE, and mice treated with PLP136-150/IFA sc were significantly protected from the subsequent induction of EAE with any peptide, while PLP139-151/IFA sc did not exert such protective effects (Fig. 9b). Moreover, the proportional increases in Tregs and their DP subset were observed in mice treated with PLP136-150/IFA sc as seen with the PLP136-150/CFA sc treatment. However, a similar increase in Tregs was not detected in mice receiving other peptide tolerance treatments, such as peptide/IFA ip (Fig. 9c). Thus, we concluded that sensitization with PLP136-150 would uniquely induce the peptide non-specific, but tissue preferential, inhibition of EAE by increasing the DP subset of Treg.

Finally, passive EAE induced by the transfer of encephalitogenic T-cells

Table 1
Analyses of the hydrogen bonds between MHC I–As and PLPs Hydrogen bonds were defined as having donor−acceptor distances <3.0 Å and a hydrogen−donor−acceptor angle <20°. Only hydrogen bonds with more than 10% occupancy are listed. In the Donor/Acceptor columns, α, β, and P represent the MHC-α chain, MHC-β chain, and PLP-peptide, respectively. Hydrogen bonds involving the PLP-peptide are in bold, and amino acid residues in MHC responsible for hydrogen bonds were underlined when the same residues were found in both the left and right columns. Most hydrogen bonds (11/13 in MHC-PLP136−150 and 12/13 in MHC-PLP139−151) were formed between MHC I–As and the main chain atoms of the PLPs, reflecting the function of MHC I–As that accommodates a wide variety of peptides.

PLP136−150			**PLP139−151**		
Donor	Acceptor	%	Donor	Acceptor	%
A:THR56-Side	**P:ARG136-Main**	11.7	A:THR56-Side	**P:HIS139-Main**	13.6
			A:THR56-Side	**P:HIS139-Side**	10.0
B:HIS106-Side	**P:VAL137-Main**	14.1	B:HIS106-Side	**P:CYS140-Main**	14.2
P:SER138-Main	A:SER57-Main	36.4	**P:LEU141-Main**	A:SER57-Main	14.6
B:ASN107-Side	**P:HIS139-Main**	44.7	B:ASN107-Side	**P:GLY142-Main**	10.9
P:HIS139-Main	B:ASN107-Side	19.6			
–	–	–	B:THR102-Side	**P:LYS143-Main**	13.6
P:LEU141-Main	A:TYR12-Main	24.3	A:TYR26-Side	**P:TRP144-Main**	10.8
			P:TRP144-Main	A:TYR12-Main	10.0
P:GLY142-Main	B:GLU99-Side	15.8	**P:LEU145-Main**	B:GLU99-Side	18.9
			P:GLY146-Main	B:GLU99-Side	15.9
P:LYS143-Side	A:THR69-Side	10.2	–	–	–
B:TYR88-Side	**P:TRP144-Main**	25.8	–	–	–
B:TYR92-Side	**P:LEU145-Main**	50.7	–	–	–
–	–	–	–	–	–
P:HIS147-Main	B:ASP84-Side	21.6	–	–	–
–	–	–	B:TYR87-Side	**P:PHE151-Main**	17.8
			A:GLN65-Side	**P:PHE151-Main**	10.4
A:TYR72-Side	**P:ASP149-Side**	19.3			
A:ARG80-Side	**P:LYS150-Main**	44.6			

primed with either PLP139-151 or PLP136-150 similarly resulted in EAE relapse without rapid recovery (Fig. 9d). The mice were highly susceptible to re-induction of EAE, which contrasted with EAE actively induced with peptide immunization (Fig. 9d). This implied that the DP subset of Tregs could not be induced via transfer of primed effector cells, but required sensitization to the peptide itself, acting as an inverse vaccination [73].

4. Discussion

Our study focused on elucidating the mechanism of individual self-antigens contributing to discrete immune responses, which might be applicable to antigen-specific therapy. The current study was initiated after observing that immunization with discrete peptides PLP136-150 and PLP139-151 induced different types of EAE in SJL/J mice, namely M-EAE and RR-EAE, respectively (Fig. 1a). Moreover, PLP136-150-primed mice exhibited complete resistance to the re-induction of EAE when immunized with any of the encephalitogenic peptides, whereas PLP139-151-primed mice remained highly susceptible (Fig. 1b). Subsequent studies revealed that these peptides have differential abilities to induce potent Tregs, which may account for these observations (Fig. 2a–c). More detailed analysis revealed that the potent Tregs, which were more efficiently induced by PLP136-150 immunization, correspond to a Treg subset, defined by the expression of both CD69 and CD103 (DP subset; Fig. 2d–g). The DP subset of Tregs, which we describe here, expanded and acted preferentially in the inflamed CNS with more stable Foxp3 expression (Fig. 2h and i). Using MHC-class II dextramer loaded with PLP139-151, we found that PLP136-150 immunization efficiently induced and maintained antigen-specific Tregs, especially composed of DP subset (Fig. 5f–h). These results were unexpected as the sequences of these two peptides differed only in their peptide flanking residues. However, the importance of peptide flanking residues was highlighted first in EAE experiments using a lower dose of peptide for immunization (Fig. 3c and d). At the 10 times lower dose, PLP136-150 induced EAE, whereas PLP139-151 was non-encephalitogenic. The results indicated that the two peptides might have qualitatively different abilities to expand cross-reactive encephalitogenic T-cells. *In vitro* experiments and *ex vivo* flow cytometric analysis (Fig. 6a, c) further implied that the numerical and functional stability of PLP-specific Tregs depended on how stably the peptide binds to I–As MHC-class II. Unexpectedly, flanking residues of the peptide had a major influence on MHC-class II binding (Fig. 8). Tregs appeared to depend on how stably the peptide binds to I–As MHC-class II.

Tregs are promising therapeutic targets for autoimmune diseases in suppressing excessive immune responses while avoiding collateral imbalance that might occur in the therapy with molecular target agents [74]. However, they have a risk for infection and tumor development by their non-specific suppression [75] and a plasticity issue that allows their conversion to pathogenic effector cells in some circumstances [76]. Functionally, Treg stability has been linked to epigenetic modifications in *Foxp3* and other Treg-signature genes [77]. These modifications, established in the thymus, are preserved with lineage continuity even in the periphery and retain stabilized suppressive functions, including inflammatory stimuli, in most circumstances [78]. However, a recent study reported that such epigenetic modifications are insufficient to secure the stability of antigen-specific Tregs under autoimmune inflammatory conditions [79,80]. In addition, Treg stability requires enhancement of TCR strength [81] or IL-2R signaling [82,83] and the acquisition of co-expression of another transcription factor to transform into effector Tregs [84], which is established to adapt to local environments [85–87]. Particularly, effector Tregs can act as tissue-resident Tregs and participate in tissue homeostasis, while in other circumstances, they become pathogenic via loss of Foxp3 expression [80, 87–89]. Their heterogeneity might explain this discrepancy. Using I–As dextramer, we revealed the presence of antigen-specific Tregs in the DP ($CD69^+CD103^+$) and 103SP ($CD69^-CD103^+$) subsets (Fig. 5f). In the DP subset, $dextramer^+$ Tregs were found exclusively in the $Foxp3^+$ fraction, whereas they were also present in the $Foxp3^-$ fraction of the 103SP subset (Fig. 5g and h). The DP subset preferentially expanded in the CNS after the EAE peak and could suppress the activation of encephalitogenic T-cells at any period of the EAE. In contrast, the 103SP subset infiltrated the CNS around the EAE peak and could mitigate and exacerbate EAE during the induction and recovery phase of EAE, respectively (Fig. 2h, g). Although both Treg subsets expressed effector signatures, the DP and 103SP subsets presented different TCR signaling patterns, cytokine profiles, and survival capacities in response to stimulation by distinct cognate antigens (manuscript in preparation). Therefore, the expansion and stabilization of the DP subset would likely require the persistent and proper presentation of the dominant peptide antigen that was naturally

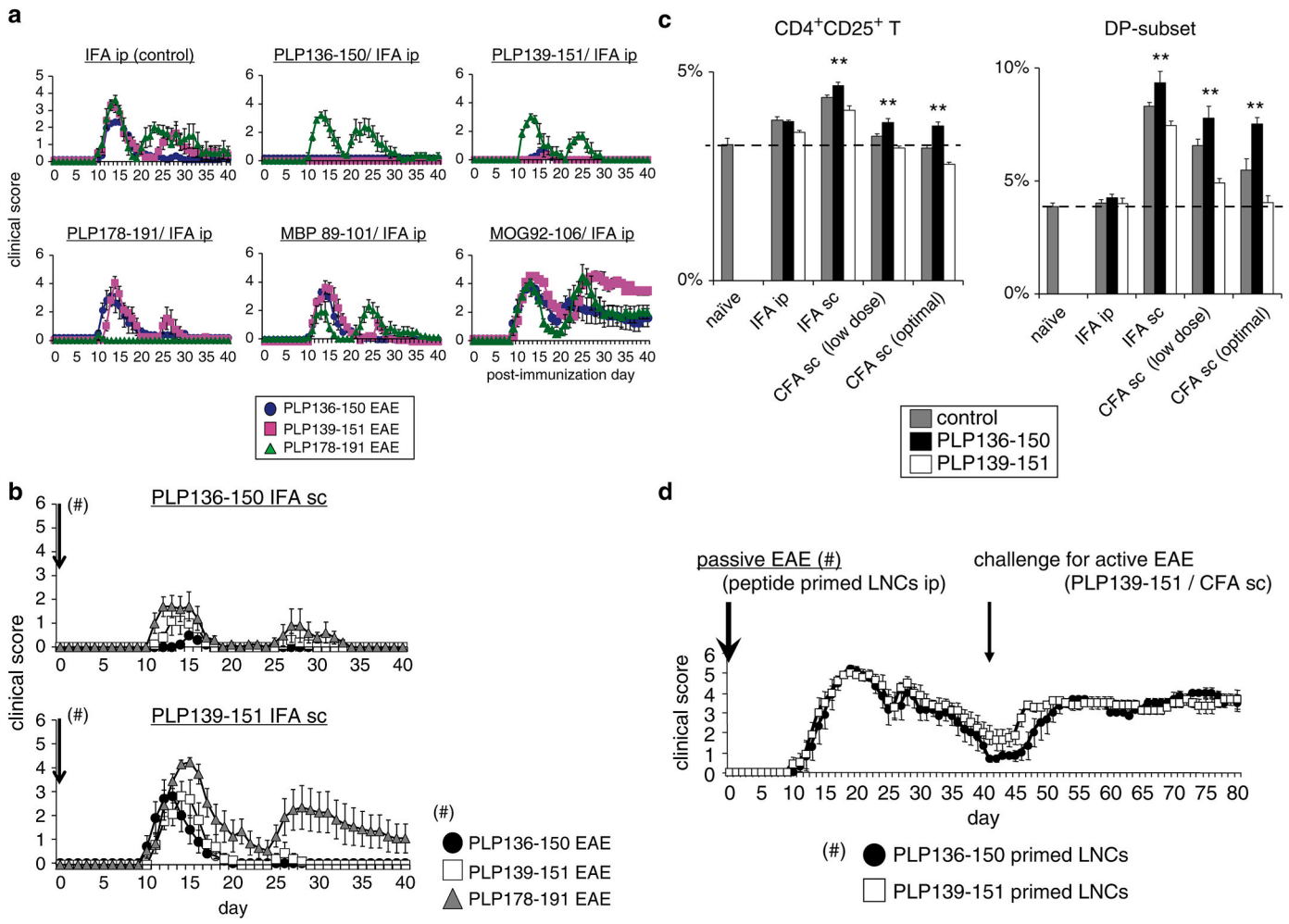

Fig. 9. Resistance to EAE re-induction via induction of Tregs required PLP136-150 immunization To confirm the effects of the PLP136-150 priming on EAE inhibition, the following three conditions: (a) routes of administration; (b) EAE development; and (d) peptide presence were evaluated. (a) Peptide tolerance was induced in SJL/J mice by intraperitoneal (ip) injection of encephalitogenic peptides (PLP136-150, PLP139-151, PLP178-191, MBP89-101, and MOG92-106) emulsified in IFA 14 days before EAE induction by immunization with PLP136-150, PLP139-151, or PLP178-191. IFA with no peptide was used as a control (n = 5 mice/group). (b) Peptide sensitization without EAE development. Mice were immunized with PLP136-150 emulsified in IFA (referred to PLP136-150/IFA) or PLP139-151/IFA subcutaneously (sc) before EAE induction by re-immunization with PLP139-151/CFA on d35. PBS/IFA used as control (n = 5 mice/group). (c) Frequency of the DP subset of $CD4^+CD25^+$ T-cells in LN from PLP-peptide-tolerant mice (referred to PLP-peptide/IFA ip) and PLP-peptide-immunized mice (referred to PLP-peptide/IFA sc or PLP-peptide/CFA sc), compared with naïve mice (*$P < 0.05$, **$P < 0.01$). (d) Passive EAE. Irradiated naïve mice were administered PLP136-150-sensitized LNs or PLP139-151-sensitized LNs on d13 for passive EAE and were then re-immunized with PLP139-151/CFA on d40 for active EAE (n = 5 mice/group).

exposed in the CNS tissue, which is similar to the activation of the tumor-infiltrating effector Tregs *in situ* [90]; otherwise, the 103SP subset was infiltrated. As such, PLP136-150 priming could secure the stability of induced Tregs as it efficiently expanded the most potent and stable DP subset. In contrast, PLP139-151 priming could not maintain the DP subset, leading to the expansion of the 103SP subset, which contained Tregs with the plasticity to differentiate into pathogenic cells.

Regarding the structural aspects, we discovered that the peptide flanking residues of PLP136-150 and PLP139-151 were key to determining their encephalitogenic potentials and ability to maintain antigen-specific Tregs (Figs. 3c and 5b, g, h, Fig. 6a and b). Given that PLP136-150 and PLP139-151 greatly differed in encephalitogenicity, conclusively with low-dose priming, it is possible that a higher functional avidity interaction of their cognate peptide with encephalitogenic T-cells may give rise to the generation of potent regulatory T-cells as well as more encephalitogenic T-cells. The high-avidity TCR-pMHC interactions tend to cause T-cell apoptosis, while apoptosis-resistant cells acquire regulatory features in human type 1 diabetes [91].

Regarding peptide avidity and potential immunogenicity, past studies using altered peptide ligands (APL) emphasized the role of the TCR contact and MHC binding residues of a given peptide [70,92]. Herein, however, we demonstrated the importance of peptide flanking residues based on the results of *in vivo* and *in silico* analysis (Figs. 6b and 8). The contributions of peptide flanking residues to enhance immunogenicity *in vitro* were reported using the egg white lysozyme (HEL) system [93,94]. Moreover, a relationship between peptide length and peptide flanking residues with binding affinity and stability has been reported [95–97]. Single-molecule X-ray analysis of the HEL peptide demonstrated that short peptides might move into the MHC groove more freely than larger peptides [98], which may generate conformational changes, leading to the induction of cryptic autoimmunity [98,99]. Our findings that peptide flanking residues directly contribute to binding stability could be regarded as proof of this assumption. The *in silico* results (Fig. 8, Video 1) indicate that higher stability of peptide binding to MHC-class II can facilitate longer contact between the TCR and peptide, thus inducing efficiently stabilized antigen-specific Tregs.

The results of the present study will have major implications on our understanding of how self-sensitization fails to be resolved in certain cases, leading to the development of chronic autoimmune diseases while succeeding in other cases. Our findings suggest the overwhelming importance

of peptide sequence for primary sensitization. As evidenced by the comparison of dominant and cryptic peptides, the responses to dominant peptides govern and simplify the subsequent reactivity to other antigens (Fig. 4). Such simplification may be advantageous for peptide selection in non-necessity to consider mixtures of multiple antigens [100], which may be generated during epitope spreading [101,102], including even unidentified ones. Moreover, as was determined from the comparison between dominant peptides (PLP136-150 and PLP139-151), which also affected the response in immunization with cryptic peptide (Fig. 3b), the preferential peptide has the potential to efficiently induce and maintain a distinct subset of efficacious antigen-specific Tregs (Fig. 2d, e, h, Fig. 5); functionally, such peptides may stimulate corresponding T-cells at a higher frequency and for a longer duration. Sensitization to the preferential dominant self-peptide should be exploited for the prevention or termination of pathogenic autoimmunity. We postulate that a current version of the suppressor determinant of the antigen will be highly immunogenic and capable of inducing potent Tregs like PLP136-150 in SJL/J mice, although the assumption was discovered in one animal strain in which several encephalitogenic peptides were identified.

Under the "immunological homunculus" paradigm, Cohen explained why natural autoimmunity is prevalent in the healthy immune system [103]. According to this concept, proper autoimmunity is expected to protect damaged tissues by preventing secondary degeneration [104,105]. Our data support this concept; that is, PLP136-150-induced M-EAE resulted in quicker recovery when compared with PLP139-151-induced RR-EAE, secondary immunization of PLP136-150 induced recovery in either PLP139-151- or PLP178-191-induced RR-EAE with progressive capacity (Fig. 1), and the lymphocytes from convalescent mice could suppress progression (Fig. 2c). We further observed the tissue repair capacity of the DP subset of Tregs in PLP136-150-immunized mice (manuscript in preparation).

Our understanding of the complexities of the immune system historically keeps pace with the study of EAE, which originated from a rare allergic reaction observed in the early vaccination era [106]. Although advanced vaccination prevents many infectious diseases, eliminating infection hygienically would likely lead to the development of autoimmune diseases [107]. Also, the recently advancing cancer immunotherapy poses risks for developing them [108]. Based on our results, we propose that preferential dominant peptides, such as PLP136-150, should be considered for antigen-specific peptide therapies to govern autoimmune diseases by inverse vaccination, achieving benign autoimmunity, whereas they should be avoided for use in peptide-based therapies as anti-tumor immunotherapies.

Funding

This work was supported by a Grant-in-Aid for Scientific Research (grant numbers 25461301, 16K09706, and 18H04045 to Y.L.); a Grant-in-Aid for Young Scientists (grant numbers 18790606 and 21790855 to Y.L.); and a Grant-in-Aid for Scientific Research on Innovative Areas (grant numbers JP19H05410 to S·S.) from Japanese Society for Promotion of Science (transfered from the Ministry of Education, Culture, Sports, Science and Technology Agency [MEXT]), Japan.

The funding sources had no involvement in study design; in the collection, analysis and interpretation of data; in the writing of the report; and in the decision to submit the article for publication.

CRediT authorship contribution statement

Youwei Lin: Conceptualization, Data curation, Funding acquisition, Investigation, Project administration, Visualization, Writing – original draft, Writing – review & editing. **Shun Sakuraba:** Investigation. **Chandirasegaran Massilamany:** Resources. **Jayagopala Reddy:** Resources. **Yoshimasa Tanaka:** Formal analysis. **Sachiko Miyake:** Conceptualization, Methodology. **Takashi Yamamura:** Conceptualization, Funding acquisition, Project administration, Supervision, Writing – review & editing.

Declaration of competing interest

The authors declare no competing financial interests.

Acknowledgments

We would like to thank Mrs. Noriko Furusawa for providing accounting support.

Appendix A. Supplementary data

Supplementary data to this article can be found online at https://doi.org/10.1016/j.jaut.2023.103094.

References

[1] Q. Leng, Z. Bentwich, Beyond self and nonself: fuzzy recognition of the immune system, Scand. J. Immunol. 56 (2002) 224–232, https://doi.org/10.1046/j.1365-3083.2002.01105.x.
[2] M. Moser, O. Leo, Key concepts in immunology, Vaccine 28 (Supplment 3) (2010) C2–C13, https://doi.org/10.1016/j.vaccine.2010.07.022.
[3] D.M. Richards, B. Kyewski, M. Feuerer, Re-examining the nature and function of self-reactive T cells, Trends Immunol. 37 (2016) 114–125, https://doi.org/10.1016/j.it.2015.12.005.
[4] J. Pol, J. Paillet, C. Plantureux, G. Kroemer, Beneficial autoimmunity and maladaptive inflammation shape epidemiological links between cancer and immune-inflammatory diseases, OncoImmunology 11 (2022), 2029299, https://doi.org/10.1080/2162402X.2022.2029299.
[5] J.H. Cho, M. Feldman, Heterogeneity of autoimmune diseases: pathophysiologic insights from genetics and implications for new therapies, Nat. Med. 21 (2015) 730–738, https://doi.org/10.1038/nm.3897.
[6] A.K. Shakya, K.S. Nandakumar, Antigen-specific tolerization and targeted delivery as therapeutic strategies for autoimmune diseases, Trends Biotechnol. 36 (2018) 686–699, https://doi.org/10.1016/j.tibtech.2018.02.008.
[7] D.E. Smilek, M.R. Ehlers, G.T. Nepom, Restoring the balance: immunotherapeutic combinations for autoimmune disease, Dis. Model. Mech. 7 (2014) 503–513, https://doi.org/10.1242/dmm.015099.
[8] K.F. Baker, J.D. Isaacs, Novel therapies for immune-mediated inflammatory diseases: what can we learn from their use in rheumatoid arthritis, spondyloarthritis, systemic lupus erythematosus, psoriasis, Crohn's disease and ulcerative colitis? Ann. Rheum. Dis. 77 (2018) 175–187, https://doi.org/10.1136/annrheumdis-2017-211555.
[9] Y. Tanaka, Recent progress in treatments of rheumatoid arthritis: an overview of developments in biologics and small molecules, and remaining unmet needs, Rheumatology 60 (Supplement 6) (2021), https://doi.org/10.1093/rheumatology/keab609 vi12–vi20.
[10] J. Sakowska, Ł. Arcimowicz, M. Jankowiak, I. Papak, A. Markiewicz, K. Dziubek, M. Kurkowiak, S. Kote, K. Kaźmierczak-Siedlecka, K. Połom, N. Marek-Trzonkowska, P. Trzonkowski, Autoimmunity and cancer—two sides of the same coin, Front. Immunol. 13 (2022), 793234, https://doi.org/10.3389/fimmu.2022.793234.
[11] A.D. Del Gatto, M. Saviano, L. Zaccaro, An overview of peptide-based molecules as potential drug candidates for multiple sclerosis, Molecules 26 (2021) 5227, https://doi.org/10.3390/molecules26175227.
[12] J. Montaño, J. Garnica, P. Santamaria, Immunomodulatory and immunoregulatory nanomedicines for autoimmunity, Semin. Immunol. 56 (2021), 101535, https://doi.org/10.1016/j.smim.2021.101535.
[13] G. Sármay, Biologia futura: emerging antigen-specific therapies for autoimmune diseases, Biol. Futur. 72 (1) (2021) 15–24, https://doi.org/10.1007/s42977-021-00074-4.
[14] C. Selck, M. Dominguez-Villar, Antigen-specific regulatory T cell therapy in autoimmune diseases and transplantation, Front. Immunol. 12 (2021), 661875, https://doi.org/10.3389/fimmu.2021.661875.
[15] C. Ballerini, Experimental autoimmune encephalomyelitis, Methods Mol. Biol. 2285 (2021) 375–384, https://doi.org/10.1007/978-1-0716-1311-5_27.
[16] E.A. Kabat, A. Wolf, A.E. Bezer, The rapid production of acute disseminated encephalomyelitis in rhesus monkeys by injection of heterologous and homologous brain tissue with adjuvants, J. Exp. Med. 85 (1946) 117–130, https://doi.org/10.1084/jem.85.1.117.
[17] I.M. Morgan, Allergic encephalomyelitis in monkeys in response to injection of normal monkey nervous tissue, J. Exp. Med. 85 (1947) 131–140, https://doi.org/10.1084/jem.85.1.131.
[18] G. Lamoureux, P. R. Carnegie, T. A. McPherson, D. Johnston, Experimental allergic encephalomyelitis: immunological properties of encephalitogenic polypeptides and proteins, Clin. Exp. Immunol. 2 (1967) 601-609.
[19] M.A. Kroenke, T.J. Carlson, A.V. Andjelkovic, B.M. Segal, IL-12- and IL-23-modulated T cells induce distinct types of EAE based on histology, CNS chemokine profile, and response to cytokine inhibition, J. Exp. Med. 205 (2008) 1535–1541, https://doi.org/10.1084/jem.20080159.
[20] N. Saligrama, F. Zhao, M.J. Sikora, W.S. Serratelli, R.A. Fernandes, D.M. Louis, W. Yao, X. Ji, J. Idoyaga, V.B. Mahajan, L.M. Steinmetz, Y.H. Chien, S.L. Hauser,

J.R. Oksenberg, K.C. Garcia, M.M. Davis, Opposing T cell responses in experimental autoimmune encephalomyelitis, Nature 572 (2019) 481–487, https://doi.org/10.1038/s41586-019-1467-x.
[21] N. Feizi, C. Focaccetti, I. Pacella, G. Tucci, A. Rossi, M. Costanza, R. Pedotti, J. Sidney, A. Sette, C. La Rocca, C. Procaccini, G. Matarese, V. Barnaba, S. Piconese, CD8+ T cells specific for cryptic apoptosis-associated epitopes exacerbate experimental autoimmune encephalomyelitis, Cell Death Dis. 12 (2021) 1026, https://doi.org/10.1038/s41419-021-04310-6.
[22] R. Gold, C. Linington, H. Lassmann, Understanding pathogenesis and therapy of multiple sclerosis via animal models: 70 years of merits and culprits in experimental autoimmune encephalomyelitis research, Brain 129 (2006) 1953–1971, https://doi.org/10.1093/brain/awl075.
[23] S.B. Simmons, E.R. Pierson, S.Y. Lee, J.M. Goverman, Modeling the heterogeneity of multiple sclerosis in animals, Trends Immunol. 34 (2013) 410–422, https://doi.org/10.1016/j.it.2013.04.006.
[24] V. K. Tuohy, R. A. Sobel, M. B. Lees, Myelin proteolipid protein-induced experimental allergic encephalomyelitis. Variations of disease expression in different strains of mice, J. Immunol. 140 (1988) 1868-1873.
[25] R. J. Butterfield, E. P. Blankenhorn, R. J. Roper, J. F. Zachary, R. W. Doerge, J. Sudweeks, J. Rose, C. Teuscher, Genetic analysis of disease subtypes and sexual dimorphisms in mouse experimental allergic encephalomyelitis (EAE): relapsing/remitting and monophasic remitting/nonrelapsing EAE are immunogenetically distinct, J. Immunol. 162 (1999) 3096-3102.
[26] I.M. Stromnes, L.M. Cerretti, D. Liggitt, R.A. Harris, J.M. Goverman, Differential regulation of central nervous system autoimmunity by T(H)1 and T(H)17 cells, Nat. Med. 14 (2008) 337–342, https://doi.org/10.1038/nm1715.
[27] J.A. Encinas, H.L. Weiner, V.K. Kuchroo, Inheritance of susceptibility to experimental autoimmune encephalomyelitis, J. Neurosci. Res. 45 (1996) 655–669, https://doi.org/10.1002/(SICI)1097-4547(19960915)45:6<655::AID-JNR2>3.0.CO;2-7.
[28] V. K. Tuohy, Z. J. Lu, R. A. Sobel, R. A. Laursen, M. B. Lees, Identification of an encephalitogenic determinant of myelin proteolipid protein for SJL mice, J. Immunol. 142 (1989) 1523-1527.
[29] I. Mendel, N. Kerlero de Rosbo, A. Ben-Nun, A myelin oligodendrocyte glycoprotein peptide induces typical chronic experimental autoimmune encephalomyelitis in H-2b mice: fine specificity and T cell receptor V beta expression of encephalitogenic T cells, Eur. J. Immunol. 25 (1995) 1951–1959, https://doi.org/10.1002/eji.1830250723.
[30] M. Endoh, T. Kunishita, J. Nihei, M. Nishizawa, T. Tabira, Susceptibility to proteolipid apoprotein and its encephalitogenic determinants in mice, Int. Arch. Allergy Appl. Immunol. 92 (1990) 433–438, https://doi.org/10.1159/000235176.
[31] J. M. Greer, V. K. Kuchroo, R. A. Sobel, M. B. Lees, Identification and characterization of a second encephalitogenic determinant of myelin proteolipid protein (residues 178-191) for SJL mice, J. Immunol. 149 (1992) 783-788.
[32] S.S. Zamvil, D.J. Mitchell, A.C. Moore, K. Kitamura, L. Steinman, J.B. Rothbard, T-cell epitope of the autoantigen myelin basic protein that induces encephalomyelitis, Nature 324 (1986) 258–260, https://doi.org/10.1038/324258a0.
[33] S. Amor, N. Groome, C. Linington, M. M. Morris, K. Dornmair, M. V. Gardinier, J. M. Matthieu, D. Baker, Identification of epitopes of myelin oligodendrocyte glycoprotein for the induction of experimental allergic encephalomyelitis in SJL and Biozzi AB/H mice, J. Immunol. 153 (1994) 4349-4356.
[34] K. Miyamoto, S. Miyake, T. Yamamura, A synthetic glycolipid prevents autoimmune encephalomyelitis by inducing Th2 bias of natural killer T cells, Nature 413 (2001) 531–534, https://doi.org/10.1038/35097097.
[35] J.W. Lindsey, Use of reinduced experimental autoimmune encephalomyelitis to evaluate the importance of epitope spread, Int. Immunol. 10 (1998) 743–748, https://doi.org/10.1093/intimm/10.6.743.
[36] T. Yamamura, T. Namikawa, M. Endoh, T. Kunishita, T. Tabira, Passive transfer of experimental allergic encephalomyelitis induced by proteolipid apoprotein, J. Neurol. Sci. 76 (1986) 269–275, https://doi.org/10.1016/0022-510X(86)90174-7.
[37] A. Chiba, S. Oki, K. Miyamoto, H. Hashimoto, T. Yamamura, S. Miyake, Suppression of collagen-induced arthritis by natural killer T cell activation with OCH, a sphingosine-truncated analog of alpha-galactosylceramide, Arthritis Rheum. 50 (2004) 305–313, https://doi.org/10.1002/art.11489.
[38] J. Reddy, E. Bettelli, L. Nicholson, H. Waldner, M.H. Jang, K.W. Wucherpfennig, V.K. Kuchroo, Detection of autoreactive myelin proteolipid protein 139–151-specific T cells by using MHC II (IAs) tetramers, J. Immunol. 170 (2003) 870–877, https://doi.org/10.4049/jimmunol.170.2.870.
[39] C. Massilamany, B. Upadhyaya, A. Gangaplara, C. Kuszynski, J. Reddy, Detection of autoreactive CD4 T cells using major histocompatibility complex class II dextramers, BMC Immunol. 12 (2011) 40, https://doi.org/10.1186/1471-2172-12-40.
[40] S. Marusić, S. Tonegawa, Tolerance induction and autoimmune encephalomyelitis amelioration after administration of myelin basic protein-derived peptide, J. Exp. Med. 186 (1997) 507–515, https://doi.org/10.1084/jem.186.4.507.
[41] J.M. Critchfield, M.K. Racke, J.C. Zúñiga-Pflücker, B. Cannella, C.S. Raine, J. Goverman, M.J. Lenardo, T cell deletion in high antigen dose therapy of autoimmune encephalomyelitis, Science 263 (1994) 1139–1143, https://doi.org/10.1126/science.7509084.
[42] A.A. Vandenbark, M. Vainiene, K. Ariail, S.D. Miller, H. Offner, Prevention and treatment of relapsing autoimmune encephalomyelitis with myelin peptide-coupled splenocytes, J. Neurosci. Res. 45 (1996) 430–438, https://doi.org/10.1002/(SICI)1097-4547(19960815)45:4<430::AID-JNR12>3.0.CO;2-4.
[43] N. Fukuhara, T. Kawabata, HOMCOS: a server to predict interacting protein pairs and interacting sites by homology modeling of complex structures, Nucleic Acids Res. 36 (Web Server issue) (2008) W185–W189, https://doi.org/10.1093/nar/gkn218.
[44] A. Fiser, A. Šali, Modeller: generation and refinement of homology-based protein structure models, Methods Enzymol. 374 (2003) 461–491, https://doi.org/10.1016/S0076-6879(03)74020-8.
[45] J.A. Maier, C. Martinez, K. Kasavajhala, L. Wickstrom, K.E. Hauser, C. Simmerling, ff14SB: improving the accuracy of protein side chain and backbone parameters from ff99SB, J. Chem. Theor. Comput. 11 (2015) 3696–3713, https://doi.org/10.1021/acs.jctc.5b00255.
[46] W.L. Jorgensen, J. Chandrasekhar, J.D. Madura, Comparison of simple potential functions for simulating liquid water, J. Chem. Phys. 79 (1983) 926–935, https://doi.org/10.1063/1.445869.
[47] I.S. Joung, T.E. Cheatham 3rd, Determination of alkali and halide monovalent ion parameters for use in explicitly solvated biomolecular simulations, J. Phys. Chem. B 112 (2008) 9020–9041, https://doi.org/10.1021/jp8001614.
[48] L. Wang, R.A. Friesner, B.J. Berne, Replica exchange with solute scaling: a more efficient version of replica exchange with solute tempering (REST2), J. Phys. Chem. B 115 (2011) 9431–9438, https://doi.org/10.1021/jp204407d.
[49] M.J. Abraham, T. Murtola, R. Schulz, S. Páll, J.C. Smith, B. Hess, E. Lindahl, GROMACS: high performance molecular simulations through multi-level parallelism from laptops to supercomputers, SoftwareX 1–2 (2015) 19–25, https://doi.org/10.1016/j.softx.2015.06.001.
[50] A. Kitao, F. Hirata, N. Gō, The effects of solvent on the conformation and the collective motions of protein: normal mode analysis and molecular dynamics simulations of melittin in water and in vacuum, Chem. Phys. 158 (1991) 447–472, https://doi.org/10.1016/0301-0104(91)87082-7.
[51] D.H. Kono, J.L. Urban, S.J. Horvath, D.G. Ando, R.A. Saavedra, L. Hood, Two minor determinants of myelin basic protein induce experimental allergic encephalomyelitis in SJL/J mice, J. Exp. Med. 168 (1) (1988) 213–227, https://doi.org/10.1084/jem.168.1.213.
[52] V. K. Tuohy, Z. J. Lu, R. A. Sobel, R. A Laursen, M. B. Lees, A synthetic peptide from myelin proteolipid protein induces experimental allergic encephalomyelitis, J. Immunol. 141 (1988) 1126-1130.
[53] S. Sakaguchi, T. Yamaguchi, T. Nomura, M. Ono, Regulatory T cells and immune tolerance, Cell 133 (2008) 775–787, https://doi.org/10.1016/j.cell.2008.05.009.
[54] S. Hori, T. Nomura, S. Sakaguchi, Control of regulatory T cell development by the transcription factor Foxp3, Science 299 (2003) 1057–1061, https://doi.org/10.1126/science.1079490.
[55] E.M. Shevach, CD4+ CD25+ suppressor T cells: more question than answers, Nat. Rev. Immunol. 2 (2002) 389–400, https://doi.org/10.1038/nri821.
[56] J. Lehmann, J. Huehn, M. de la Rosa, F. Maszyna, U. Kretschmer, V. Krenn, M. Brunner, A. Scheffold, A. Hamann, Expression of the integrin alpha Ebeta 7 identifies unique subsets of $CD25^+$ as well as $CD25^-$ regulatory T cells, Proc. Natl. Acad. Sci. U.S.A. 99 (2002) 13031–13036, https://doi.org/10.1073/pnas.192162899.
[57] J. Huehn, K. Siegmund, J.C.U. Lehmann, C. Siewert, U. Haubold, M. Feuerer, G. F. Debes, J. Lauber, O. Frey, G.K. Przybylski, U. Niesner, M. de la Rosa, C. A. Schmidt, R. Bräuer, J. Buer, A. Scheffold, A. Hamann, Developmental stage, phenotype, and migration distinguish naive- and effector/memory-like $CD4^+$ regulatory T cells, J. Exp. Med. 199 (2004) 303–313, https://doi.org/10.1084/jem.20031562.
[58] D. Sancho, M. Gómez, F. Sánchez-Madrid, CD69 is an immunoregulatory molecule induced following activation, Trends Immunol. 26 (2005) 136–140, https://doi.org/10.1016/j.it.2004.12.006.
[59] D. Sancho, M. Gómez, F. Viedma, E. Esplugues, M. Gordón-Alonso, M.A. García-López, H. de la Fuente, C. Martínez-A, P. Lauzurica, F. Sánchez-Madrid, CD69 downregulates autoimmune reactivity through active transforming growth factor-beta production in collagen-induced arthritis, J. Clin. Invest. 112 (2003) 872–882, https://doi.org/10.1172/JCI19112.
[60] K. Nakamura, A. Kitani, I. Fuss, A. Pedersen, N. Harada, H. Nawata, W. Strober, TGF-beta 1 plays an important role in the mechanism of $CD4^+CD25^+$ regulatory T cell activity in both humans and mice, J. Immunol. 172 (2004) 834–842, https://doi.org/10.4049/jimmunol.172.2.834.
[61] M.J. McGeachy, L.A. Stephens, S.M. Anderton, Natural recovery and protection from autoimmune encephalomyelitis: contribution of $CD4^+CD25^+$ regulatory cells within the central nervous system, J. Immunol. 175 (2005) 3025–3032, https://doi.org/10.4049/jimmunol.175.5.3025.
[62] Y. Liu, I. Teige, B. Birnir, S. Issazadeh-Navikas, Neuron-mediated generation of regulatory T cells from encephalitogenic T cells suppress EAE, Nat. Med. 12 (2006) 518–525, https://doi.org/10.1038/nm1402.
[63] T. Korn, J. Reddy, W. Gao, E. Bettelli, A. Awasthi, T.R. Petersen, B.T. Bäckström, R.A. Sobel, K.W. Wucherpfennig, T.B. Strom, M. Oukka, V.K. Kuchroo, Myelin-specific regulatory T cells accumulate in the CNS but fail to control autoimmune inflammation, Nat. Med. 13 (2007) 423–431, https://doi.org/10.1038/nm1564.
[64] R. H. Whitham, D. N. Bourdette, G. A. Hashim, R. M. Herndon, R. C. Ilg, A. A. Vandenbark, H. Offner, Lymphocytes from SJL/J mice immunized with spinal cord respond selectively to a peptide of proteolipid protein and transfer relapsing demyelinating experimental autoimmune encephalomyelitis, J. Immunol. 146 (1991) 101-107.
[65] B. Bielekova, M.H. Sung, N. Kadom, R. Simon, H. McFarland, R. Martin, Expansion and functional relevance of high-avidity myelin-specific CD4+ T cells

in multiple sclerosis, J. Immunol. 172 (2004) 3893–3904, https://doi.org/10.4049/jimmunol.172.6.3893.
[66] S.E. Allan, S.Q. Crome, N.K. Crellin, L. Passerini, T.S. Steiner, R. Bacchetta, M. G. Roncarolo, M.K. Levings, Activation-induced FOXP3 in human T effector cells does not suppress proliferation or cytokine production, Int. Immunol. 19 (2007) 345–354, https://doi.org/10.1093/intimm/dxm014.
[67] V. K. Kuchroo, J. M. Greer, D. Kaul, G. Ishioka, A. Franco, A. Sette, R. A. Sobel, M. B. Lees, A single TCR antagonist peptide inhibits experimental allergic encephalomyelitis mediated by a diverse T cell repertoire, J. Immunol. 153 (1994) 3326-3336.
[68] M. Kalbus, B.T. Fleckenstein, M. Offenhäusser, M. Blüggel, A. Melms, H.E. Meyer, H.G. Rammensee, R. Martin, G. Jung, N. Sommer, Ligand motif of the autoimmune disease-associated mouse MHC class II molecule H2-As, Eur. J. Immunol. 31 (2001) 551–562, https://doi.org/10.1002/1521-4141(200102)31:2<551::AID-IMMU551>3.0.CO;2-P.
[69] R.C. van der Veen, P.J. Chen, M. McMillan, Myelin proteolipid protein-induced Th1 and Th2 clones express TCR with similar fine specificity for peptide and CDR3 homology despite diverse Vβ usage, Cell. Immunol. 166 (1995) 291–295, https://doi.org/10.1006/cimm.1995.9968.
[70] M.P. Das, L.B. Nicholson, J.M. Greer, V.K. Kuchroo, Autopathogenic T helper cell type 1 (Th1) and protective Th2 clones differ in their recognition of the autoantigenic peptide of myelin proteolipid protein, J. Exp. Med. 186 (1997) 867–876, https://doi.org/10.1084/jem.186.6.867.
[71] C. C. Whitacre, I. E. Gienapp, C. G. Orosz, D. M. Bitar, Oral tolerance in experimental autoimmune encephalomyelitis. III. Evidence for clonal anergy, J. Immunol. 147 (1991) 2155-2163.
[72] S.D. Miller, L.J. Tan, L. Pope, B.L. McRae, W.J. Karpus, Antigen-specific tolerance as a therapy for experimental autoimmune encephalomyelitis, Int. Rev. Immunol. 9 (1992) 203–222, https://doi.org/10.3109/08830189209061791.
[73] L. Steinman, Inverse vaccination, the opposite of Jenner's concept, for therapy of autoimmunity, J. Intern. Med. 267 (2010) 441–451, https://doi.org/10.1111/j.1365-2796.2010.02224.x.
[74] S. Sakaguchi, N. Mikami, J.B. Wing, A. Tanaka, K. Ichiyama, N. Ohkura, Regulatory T cells and human disease, Annu. Rev. Immunol. 38 (2020) 541–566, https://doi.org/10.1146/annurev-immunol-042718-041717.
[75] A. Hatzioannou, A. Boumpas, M. Papadopoulou, I. Papafragkos, A. Varveri, T. Alissafi, P. Verginis, Regulatory T cells in autoimmunity and cancer: a duplicitous lifestyle, Front. Immunol. 12 (2021), 731947, https://doi.org/10.3389/fimmu.2021.731947.
[76] X. Zhou, S. Bailey-Bucktrout, L.T. Jeker, J.A. Bluestone, Plasticity of CD4(+) FoxP3(+) T cells, Curr. Opin. Immunol. 21 (2009) 281–285, https://doi.org/10.1016/j.coi.2009.05.007.
[77] N. Ohkura, M. Hamaguchi, H. Morikawa, K. Sugimura, A. Tanaka, Y. Ito, M. Osaki, Y. Tanaka, R. Yamashita, N. Nakano, J. Huehn, H.J. Fehling, T. Sparwasser, K. Nakai, S. Sakaguchi, T cell receptor stimulation-induced epigenetic changes and Foxp3 expression are independent and complementary events required for Treg cell development, Immunity 37 (2012) 785–799, https://doi.org/10.1016/j.immuni.2012.09.010.
[78] Y.P. Rubtsov, R.E. Niec, S. Josefowicz, L. Li, J. Darce, D. Mathis, C. Benoist, A. Y. Rudensky, Stability of the regulatory T cell lineage in vivo, Science 329 (2010) 1667–1671, https://doi.org/10.1126/science.1191996.
[79] X. Zhou, S.L. Bailey-Bucktrout, L.T. Jeker, C. Penaranda, M. Martínez-Llordella, M. Ashby, M. Nakayama, W. Rosenthal, J.A. Bluestone, Instability of the transcription factor Foxp3 leads to the generation of pathogenic memory T cells in vivo, Nat. Immunol. 10 (2009) 1000–1007, https://doi.org/10.1038/ni.1774.
[80] S.L. Bailey-Bucktrout, M. Martinez-Llordella, X. Zhou, B. Anthony, W. Rosenthal, H. Luche, H.J. Fehling, J.A. Bluestone, Self-antigen-driven activation induces instability of regulatory T cells during an inflammatory autoimmune response, Immunity 39 (2013) 949–962, https://doi.org/10.1016/j.immuni.2013.10.016.
[81] E. Wakamatsu, H. Omori, A. Kawano, S. Ogawa, R. Abe, Strong TCR stimulation promotes the stabilization of Foxp3 expression in regulatory T cells induced in vitro through increasing the demethylation of Foxp3 CNS2, Biochem. Biophys. Res. Commun. 503 (2018) 2597–2602, https://doi.org/10.1016/j.bbrc.2018.07.021.
[82] V.S. Nair, K.I. Oh, Down-regulation of Tet2 prevents TSDR demethylation in IL2 deficient regulatory T cells, Biochem. Biophys. Res. Commun. 450 (2014) 918–924, https://doi.org/10.1016/j.bbrc.2014.06.110.
[83] K. Someya, H. Nakatsukasa, M. Ito, T. Kondo, K.I. Tateda, T. Akanuma, I. Koya, T. Sanosaka, J. Kohyama, Y.I. Tsukada, T. Takamura-Enya, A. Yoshimura, Improvement of Foxp3 stability through CNS2 demethylation by TET enzyme induction and activation, Int. Immunol. 29 (2017) 365–375, https://doi.org/10.1093/intimm/dxx049.
[84] E. Cretney, A. Xin, W. Shi, M. Minnich, F. Masson, M. Miasari, G.T. Belz, G. K. Smyth, M. Busslinger, S.L. Nutt, A. Kallies, The transcription factors Blimp-1 and IRF4 jointly control the differentiation and function of effector regulatory T cells, Nat. Immunol. 12 (2011) 304–311, https://doi.org/10.1038/ni.2006.
[85] J.B. Wing, S. Sakaguchi, Multiple Treg suppressive modules and their adaptability, Front. Immunol. 3 (178) (2012), https://doi.org/10.3389/fimmu.2012.00178.
[86] A. Vasanthakumar, Y. Liao, P. Teh, M.F. Pascutti, A.E. Oja, A.L. Garnham, R. Gloury, J.C. Tempany, T. Sidwell, E. Cuadrado, P. Tuijnenburg, T.W. Kuijpers, N. Lalaoui, L.A. Mielke, V.L. Bryant, P.D. Hodgkin, J. Silke, G.K. Smyth, M. A. Nolte, W. Shi, A. Kallies, The TNF receptor superfamily-NF-κB axis is critical to maintain effector regulatory T cells in lymphoid and non-lymphoid tissues, Cell Rep. 20 (2017) 2906–2920, https://doi.org/10.1016/j.celrep.2017.08.068.
[87] T. Korn, A. Muschaweckh, Stability and maintenance of Foxp3+ Treg cells in non-lymphoid microenvironments, Front. Immunol. 10 (2019) 2634, https://doi.org/10.3389/fimmu.2019.02634.
[88] M. Panduro, C. Benoist, D. Mathis, Tissue Tregs, Annu. Rev. Immunol. 34 (2016) 609–633, https://doi.org/10.1146/annurev-immunol-032712-095948.
[89] M. Dominguez-Villar, D.A. Hafler, Regulatory T cells in autoimmune disease, Nat. Immunol. 19 (2018) 665–673, https://doi.org/10.1038/s41590-018-0120-4.
[90] H. Nishikawa, S. Sakaguchi, Regulatory T cells in cancer immunotherapy, Curr. Opin. Immunol. 27 (2014) 1–7, https://doi.org/10.1016/j.coi.2013.12.005.
[91] R. Mallone, S.A. Kochik, H. Reijonen, B. Carson, S.F. Ziegler, W.W. Kwok, G. T. Nepom, Functional avidity directs T-cell fate in autoreactive CD4 T cells, Blood 106 (2005) 2798–2805, https://doi.org/10.1182/blood-2004-12-4848.
[92] L.B. Nicholson, J.M. Greer, R.A. Sobel, M.B. Lees, V.K. Kuchroo, An altered peptide ligand mediates immune deviation and prevents autoimmune encephalomyelitis, Immunity 3 (1995) 397–405, https://doi.org/10.1016/1074-7613(95)90169-8.
[93] R.T. Carson, K.M. Vignali, D.L. Woodland, D.A.A. Vignali, T cell receptor recognition of MHC class II–bound peptide flanking residues enhances immunogenicity and results in altered TCR V region usage, Immunity 7 (1997) 387–399, https://doi.org/10.1016/S1074-7613(00)80360-X.
[94] P.Y. Arnold, N.L. La Gruta, T. Miller, K.M. Vignali, P.S. Adams, D.L. Woodland, D. A.A. Vignali, The majority of immunogenic epitopes generate CD4+ T cells that are dependent on MHC class II-bound peptide-flanking residues, J. Immunol. 169 (2002) 739–749, https://doi.org/10.4049/jimmunol.169.2.739.
[95] C.A. Nelson, S.J. Petzold, E.R. Unanue, Peptides determine the lifespan of MHC class II molecules in the antigen-presenting cell, Nature 371 (1994) 250–252, https://doi.org/10.1038/371250a0.
[96] C. O'Brien, D.R. Flower, C. Feighery, Peptide length significantly influences in vitro affinity for MHC class II molecules, Immunome Res. 4 (2008) 6, https://doi.org/10.1186/1745-7580-4-6.
[97] C.J. Holland, D.K. Cole, A. Godkin, Re-directing CD4(+) T cell responses with the flanking residues of MHC class II-bound peptides- the core is not enough, Front. Immunol. 4 (2013) 172, https://doi.org/10.3389/fimmu.2013.00172.
[98] H. Kozono, Y. Matsushita, N. Ogawa, Y. Kozono, T. Miyabe, H. Sekiguchi, K. Ichiyanagi, N. Okimoto, M. Taiji, O. Kanagawa, Y.C. Sasaki, Single-molecule motions of MHC class II rely on bound peptides, Biophys. J. 108 (2015) 350–359, https://doi.org/10.1016/j.bpj.2014.12.004.
[99] J.F. Mohan, E.R. Unanue, Unconventional recognition of peptides by T cells and the implications for autoimmunity, Nat. Rev. Immunol. 12 (2012) 721–728, https://doi.org/10.1038/nri3294.
[100] J. Derdelinckx, P. Cras, Z.N. Berneman, N. Cools, Antigen-specific treatment modalities in MS: the past, the present, and the future, Front. Immunol. 12 (2021), 624685, https://doi.org/10.3389/fimmu.2021.624685.
[101] C.L. Vanderlugt, S.D. Miller, Epitope spreading in immune-mediated diseases: implications for immunotherapy, Nat. Rev. Immunol. 2 (2002) 85–95, https://doi.org/10.1038/nri724.
[102] E.J. McMahon, S.L. Bailey, C.V. Castenada, H. Waldner, S.D. Miller, Epitope spreading initiates in the CNS in two mouse models of multiple sclerosis, Nat. Med. 11 (2005) 335–339, https://doi.org/10.1038/nm1202.
[103] I.R. Cohen, D.B. Young, Autoimmunity, microbial immunity and the immunological homunculus, Immunol. Today 12 (1991) 105–110, https://doi.org/10.1016/0167-5699(91)90093-9.
[104] I.R. Cohen, M. Schwartz, Autoimmune maintenance of neuroprotection of the central nervous system, J. Neuroimmunol. 100 (1999) 111–114, https://doi.org/10.1016/S0165-5728(99)00190-3.
[105] M. Schwartz, I.R. Cohen, Autoimmunity can benefit self-maintenance, Immunol. Today 21 (2000) 265–268, https://doi.org/10.1016/S0167-5699(00)01633-9.
[106] T.M. Rivers, D.H. Sprunt, G.P. Berry, Observations on attempts to produce acute disseminated encephalomyelitis in monkeys, J. Exp. Med. 58 (1933) 39–53, https://doi.org/10.1084/jem.58.1.39.
[107] J.F. Bach, The hygiene hypothesis in autoimmunity: the role of pathogens and commensals, Nat. Rev. Immunol. 18 (2018) 105–120, https://doi.org/10.1038/nri.2017.111.
[108] K.M. Dhodapkar, Autoimmune complications of cancer immunotherapy, Curr. Opin. Immunol. 61 (2019) 54–59, https://doi.org/10.1016/j.coi.2019.08.004.

Abbreviations

69SP: $CD69^{+}CD103^{-}$ Tregs
103SP: $CD69^{-}CD103^{+}$ Tregs
CIA: collagen-induced arthritis
CNS: central nervous system
DN: $CD69^{-}CD103^{-}$ Tregs
DP: $CD69^{+}CD103^{+}$ Tregs
EAE: experimental autoimmune encephalomyelitis
LN: lymph node
MD: molecular dynamics
M-EAE: monophasic EAE
MHC: major histocompatibility complex
REST2: Replica Exchange with Solute Tempering 2
RR-EAE: relapsing-remitting EAE
TCR: T-cell receptor
Tregs: regulatory T-cells

補足資料(Supplementary data)について

ダウンロード先：https://doi. org/10.1016/j.jaut.2023.103094

内容：Sup FigS1.tif

Sup FigS2.tif

Sup FigS3.tif

Sup FigS4.tif

Sup FigS5.tif

Supporting Information.docx

Video 1.mp4

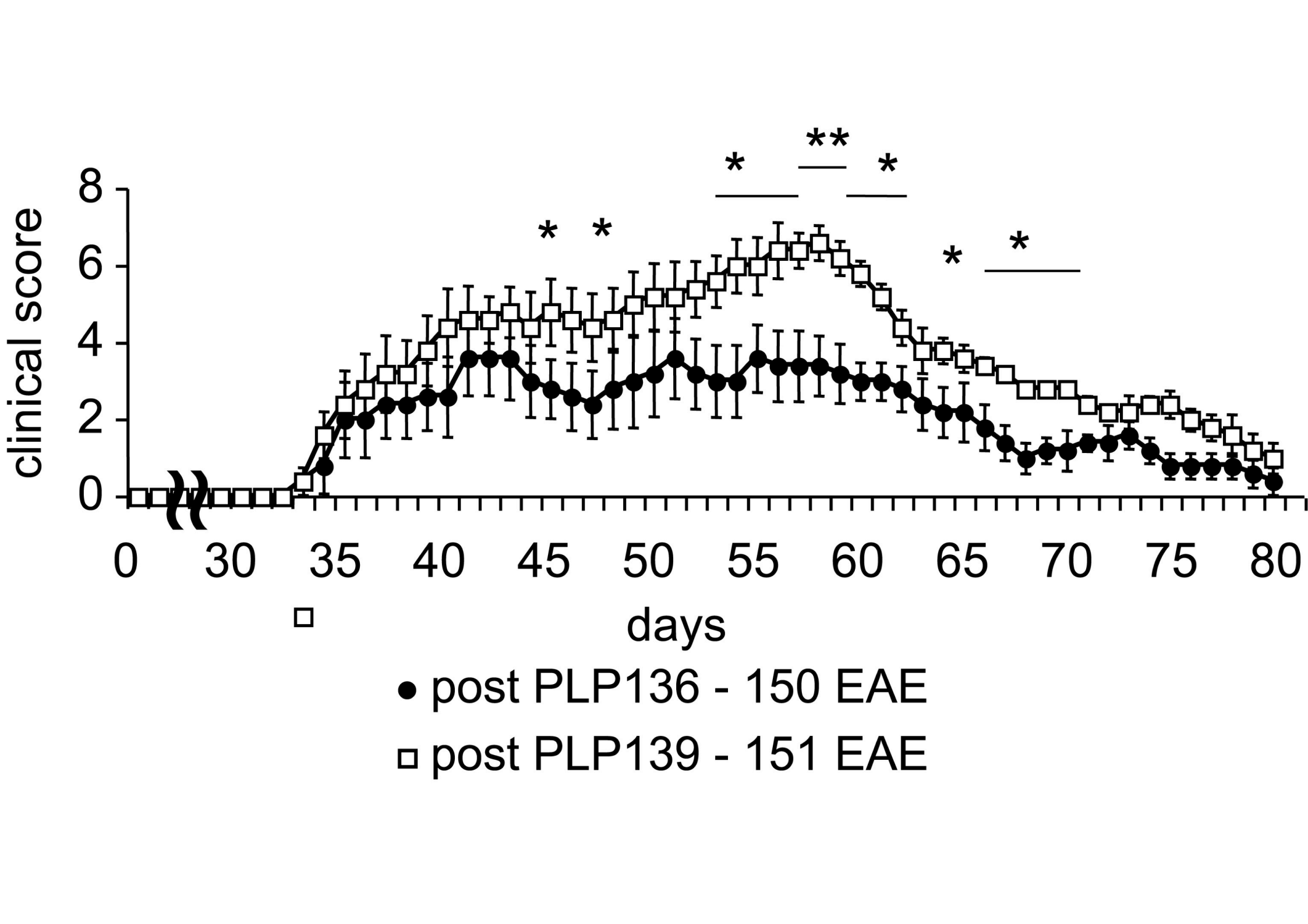
clinical score
0
2
4
6
8
0
30
35
40
45
50
55
60
65
70
75
80
days
post PLP136 - 150 EAE
post PLP139 - 151 EAE
*
*
**
*
*
*
*

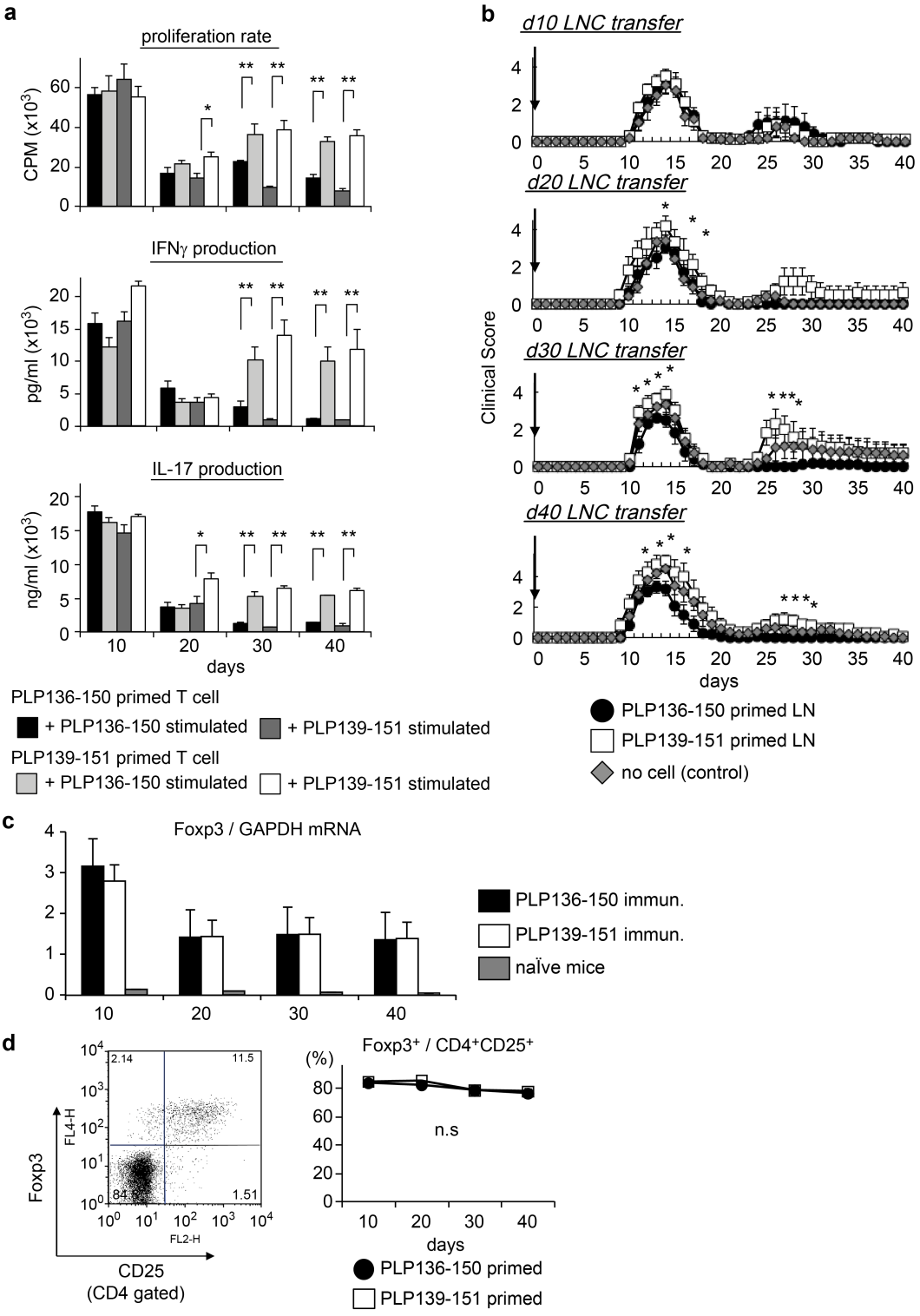
a
proliferation rate
CPM (x10³)
IFNγ production
pg/ml (x10³)
IL-17 production
ng/ml (x10³)
days
PLP136-150 primed T cell
+ PLP136-150 stimulated
+ PLP139-151 stimulated
PLP139-151 primed T cell
+ PLP136-150 stimulated
+ PLP139-151 stimulated
b
d10 LNC transfer
d20 LNC transfer
d30 LNC transfer
d40 LNC transfer
Clinical Score
days
PLP136-150 primed LN
PLP139-151 primed LN
no cell (control)
c
Foxp3 / GAPDH mRNA
PLP136-150 immun.
PLP139-151 immun.
naïve mice
d
Foxp3
CD25
(CD4 gated)
FL4-H
FL2-H
2.14
11.5
84
1.51
Foxp3⁺ / CD4⁺CD25⁺
(%)
n.s
days
PLP136-150 primed
PLP139-151 primed

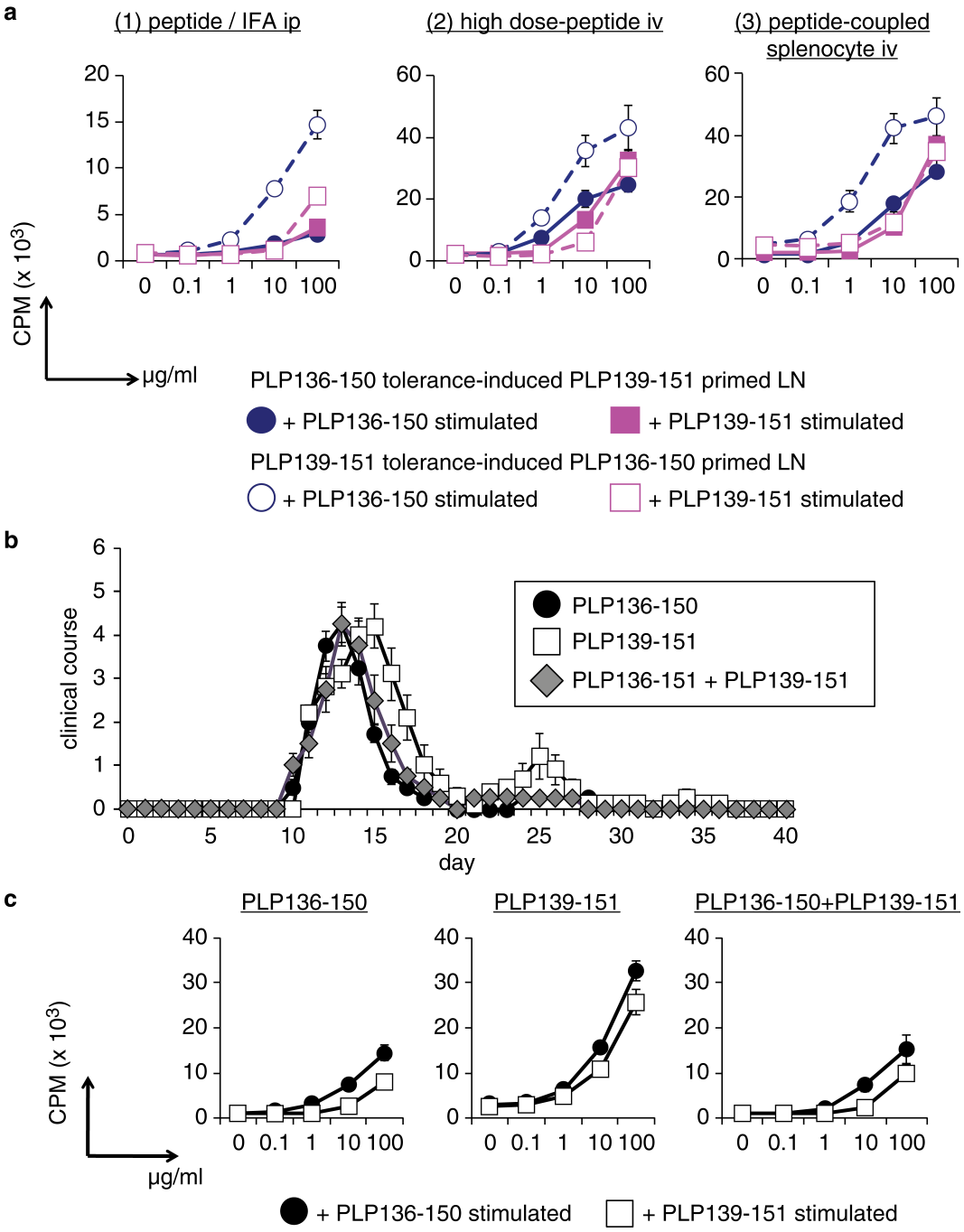
a
(1) peptide / IFA ip
(2) high dose-peptide iv
(3) peptide-coupled splenocyte iv
CPM (x 10³)
µg/ml
PLP136-150 tolerance-induced PLP139-151 primed LN
+ PLP136-150 stimulated
+ PLP139-151 stimulated
PLP139-151 tolerance-induced PLP136-150 primed LN
+ PLP136-150 stimulated
+ PLP139-151 stimulated
b
clinical course
day
PLP136-150
PLP139-151
PLP136-151 + PLP139-151
c
PLP136-150
PLP139-151
PLP136-150+PLP139-151
CPM (x 10³)
µg/ml
+ PLP136-150 stimulated
+ PLP139-151 stimulated

a

```
I-AS-a     1 EDDIEADHVGVYGTTVYQSPGDIGQYTHEFDGDEWFYVDLDKKETIWMLP   50
                |||||||.||.|||||||||||||.||||||.||||||||||:||||
1iak-a     1 ---IEADHVGSYGITVYQSPGDIGQYTFEFDGDELFYVDLDKKETVWMLP   47

I-AS-a    51 EFGQLTSFDPQGGLQNIATGKYTLGILTKRSNSTPATNEAPQATVFPKSP  100
             ||.||..|:|||||||||||||:.|.|||||||||||||||||||||||||
1iak-a    48 EFAQLRRFEPQGGLQNIATGKHNLEILTKRSNSTPATNEAPQATVFPKSP   97

I-AS-a   101 VLLGQPNTLICFVDNIFPPVINITWLRNSKSVTDGVYETSFLVNRDHSFH  150
             |||||||||||||||||||||||||||||||||||||||||.||||:|||
1iak-a    98 VLLGQPNTLICFVDNIFPPVINITWLRNSKSVTDGVYETSFFVNRDYSFH  147

I-AS-a   151 KLSYLTFIPSDDDIYDCKVEHWGLEEPVLKHWEPEIPAPMSELTE        195
             |||||||||||||||||||||||||||||||||
1iak-a    148 KLSYLTFIPSDDDIYDCKVEHWGLEEPVLKHWEPE----------       182


I-AS-b     1 GDSERHFVFQFKGECYFTNGTQRIRSVDRYIYNREEYLRFDSDVGEYRAV   50
               ..||.||:..||||||||||.|.|||||||:||||||||||||
1iak-b     1 ----GSFVHQFQPFCYFTNGTQRIRLVIRYIYNREEYVRFDSDVGEYRAV   46

I-AS-b    51 TELGRPDAEYYNKQYLEQTRAELDTVCRHNYEGVETHTSLRRLEQPNVVI  100
             ||||||||||:||||||:||||||||||||||..||.|||||||||:|||
1iak-b    47 TELGRPDAEYWNKQYLERTRAELDTVCRHNYEKTETPTSLRRLEQPSVVI   96

I-AS-b   101 SLSRTEALNHHNTLVCSVTDFYPAKIKVRWFRNGQEETVGVSSTQLISNG  150
             ||||||||||||||||||||||||||||||||||||||||||||||||.||
1iak-b    97 SLSRTEALNHHNTLVCSVTDFYPAKIKVRWFRNGQEETVGVSSTQLIRNG  146

I-AS-b   151 DWTFQVLVMLEMTPRRGEVYTCHVEHPSLKSPITVEWRAQSESARSK      197
             |||||||||||||||||||||||||||||.|||||||||
1iak-b    147 DWTFQVLVMLEMTPRRGEVYTCHVEHPSLTSPITVEWRA--------      185
```

b

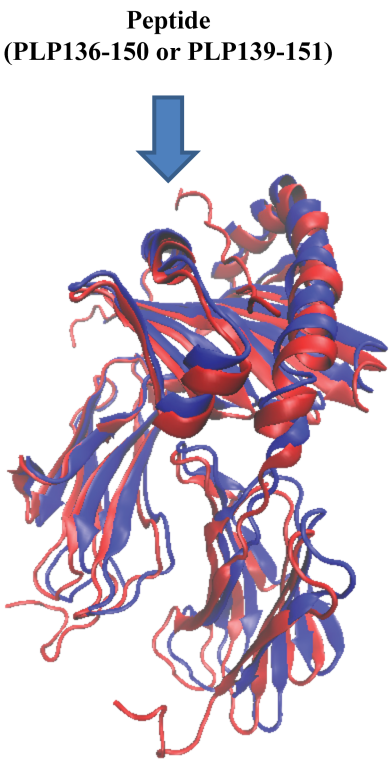

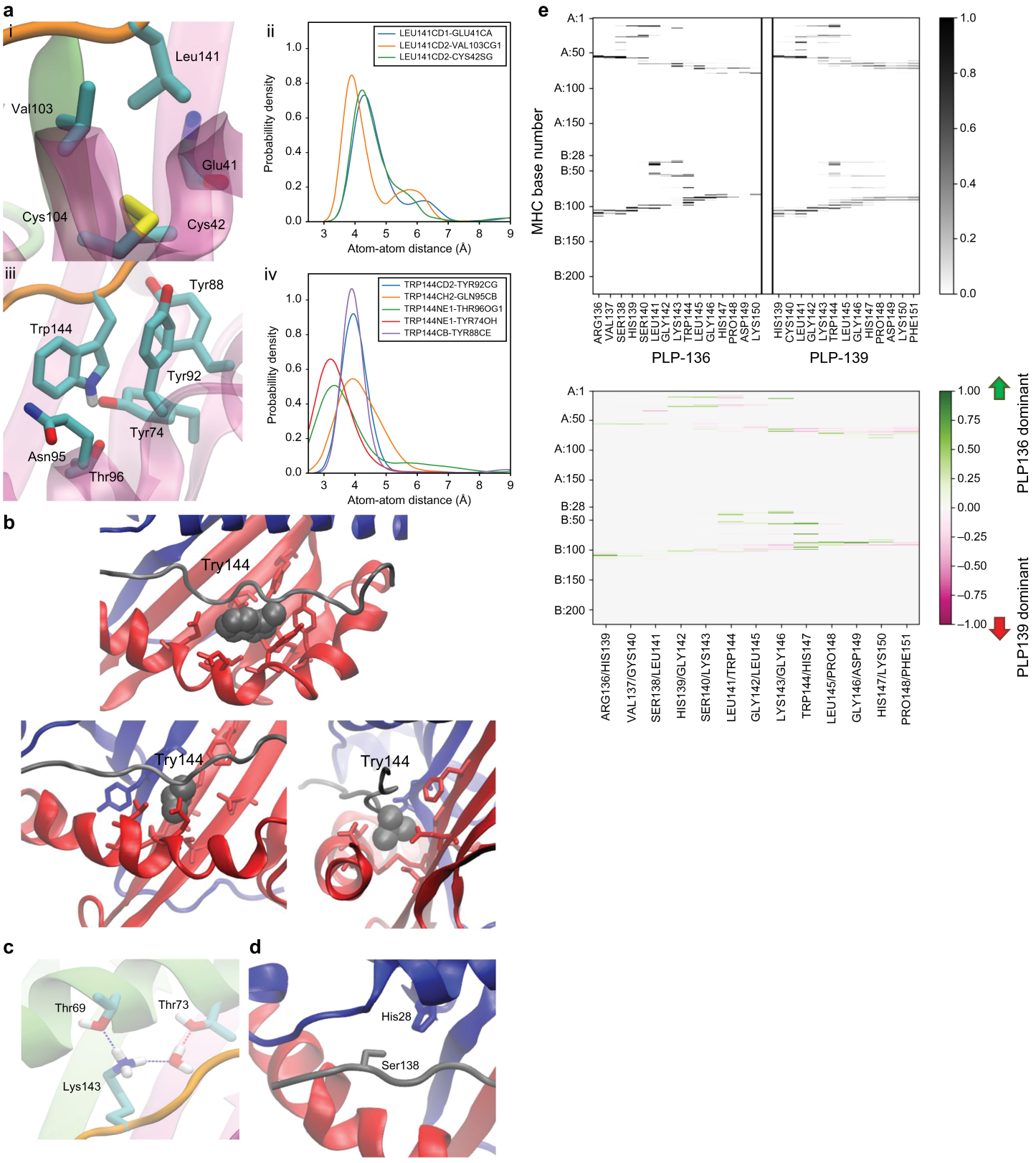
a
i
Leu141
Val103
Glu41
Cys104
Cys42
ii
LEU141CD1-GLU41CA
LEU141CD2-VAL103CG1
LEU141CD2-CYS42SG
Probability density
Atom-atom distance (Å)
iii
Tyr88
Trp144
Tyr92
Tyr74
Asn95
Thr96
iv
TRP144CD2-TYR92CG
TRP144CH2-GLN95CB
TRP144NE1-THR96OG1
TRP144NE1-TYR74OH
TRP144CB-TYR88CE
Probability density
Atom-atom distance (Å)
b
Try144
Try144
Try144
c
Thr69
Thr73
Lys143
d
His28
Ser138
e
MHC base number
A:1
A:50
A:100
A:150
B:28
B:50
B:100
B:150
B:200
ARG136 VAL137 SER138 HIS139 SER140 LEU141 GLY142 LYS143 TRP144 LEU145 GLY146 HIS147 PRO148 ASP149 LYS150
HIS139 CYS140 LEU141 GLY142 LYS143 TRP144 LEU145 GLY146 HIS147 PRO148 ASP149 LYS150 PHE151
PLP-136
PLP-139
PLP136 dominant
PLP139 dominant
ARG136/HIS139
VAL137/GYS140
SER138/LEU141
HIS139/GLY142
SER140/LYS143
LEU141/TRP144
GLY142/LEU145
LYS143/GLY146
TRP144/HIS147
LEU145/PRO148
GLY146/ASP149
HIS147/LYS150
PRO148/PHE151

Supporting Information

Detailed protocol of MHC class-II I-As simulation

The initial structure of MHC I-As molecule was refined using molecular dynamics simulation. Detailed system setups for computation are as follows. All histidine residues were modeled as HIE (protonated at Hε atoms). Six cysteine residues in MHC I-As were appropriately connected through three S-S bonds. All N- and C-termini were not capped, i.e., termini were ionic. Waters were added with the solvation thickness of at least 10 Å. There were 107,087 and 115,731 atoms for MHC-PLP136–150 and MHC-PLP139–151 systems, respectively. The simulation topology was constructed with AmberTools [AMBER] and converted to GROMACS [GMX, GMX5.1] through *acpype* [acpype].

In molecular dynamics simulation, smooth particle-mesh Ewald (PME) method [EssmanSPME] was used to evaluate long-range electrostatic interactions. The real-space electrostatic interaction of the PME, and the Lennard-Jones terms of the non-bonded interaction was cut-off at 10Å. Bonds between hydrogens and heavy atoms were constrained to be constant using P-LINCS [P-LINCS]. The integration time step was set to 2 fs. Rigid body motion of TIP3P waters were treated by SETTLE.[SETTLE] Constant temperature simulation at 300 K was achieved by employing the Langevin dynamics. The pressure was kept at 1 atm using Berendsen's barostat [BerendsenWeakScaling], and the pressure tensor was corrected by the dispersion correction scheme. The double precision version of GROMACS was used.

Brief introduction to REST2 simulation

As described in Materials and Methods, REST2 simulation was employed to sample various configurations of MHC I-As–PLP complexes. The principle of REST2 simulation is as follows. In REST2, N multiple simulations ("replicas") are performed in parallel (numbered from 0 to $N-1$). Each replica uses different potential function to sample different configurations. Specifically, the potential function U is split into three terms, namely;

$$U = U_{\mathrm{pp}} + U_{\mathrm{pw}} + U_{\mathrm{ww}}.$$

Here, "p" is the region whose sampling needs to be accelerated (named after "protein" in Ref. [REST2]), whereas "w" is the region that does not have to be accelerated (named after "water"). The potential function U_{pp} represents the interaction within the "p" region, whereas U_{pw} and U_{ww} represent those between "p" and "w" and within "w", respectively. The potential function U_m used in replica m $(0 \leq m \leq N-1)$ is then

formed as;

$$U_m = \frac{\beta_m}{\beta_0} U_{\mathrm{pp}} + \sqrt{\frac{\beta_m}{\beta_0}} U_{\mathrm{pw}} + U_{\mathrm{ww}},$$

where $\beta_m = (k_B T_m)^{-1}$, k_B=Boltzmann constant, and T_m=specified temperature. T_0 is the temperature of our interest (in this study, T_0=300 K). Simulations with high T_m allows to sample a wide variety of configurations in the accelerated regions due to weakened interactions in U_{pp} and U_{pw}. All simulations in REST2 are carried out at temperature T_0 irrespective to T_m; T_m values are used only to determine the potential function of replica m. During the simulation, at regular interval, two neighboring replicas numbered m and $m+1$ exchange their coordinates with the following probability [HamiltonianReplica] ;

$$\Pr(m, X_m, X_{m+1}) = \min\big(1, exp\big[-\beta_0\big(U_m(X_{m+1}) + U_{m+1}(X_m) - U_m(X_m) - U_{m+1}(X_{m+1})\big)\big]\big),$$

where $U_m(X_n)$ is the potential energy of particles with the coordinate in nth replica, evaluated by mth replica's potential function. With this scheme, the configurations sampled in replica 0 converges to the samples at temperature T_0. Figure S2 is a schematic representation of state exchanges between replicas. In the present study, we used N = 24 replicas and the temperatures were set to

$$T_m = \left(T_0^{-1} - \frac{m}{N-1}(T_0^{-1} - T_{N-1}^{-1})\right)^{-1},$$

where T_{N-1} was set to 600K. Neighboring replicas were exchanged every 1000 steps (i.e., 2 ps). The exchange ratios were between 35% and 54%. The distance between the center of mass of the peptide and the center of mass of the MHC cleft was restricted so as not to exceed 15 Å, by adding a flat-bottom harmonic restraint potential with the force constant of 1000 kJ mol^{-1} nm^{-2}. In the present simulation, there were no snapshots violating this distance restraint in replica 0. After 100 ns of equilibration, the convergence of 100 ns production run was observed. The trajectories were split into 10 sections (10 ns each), and the forward and backward averages of peptide Cα atom coordinates were calculated. The deviations of these time-sliced averages were all within the standard deviation among 100 ns, showing that the systems were well equilibrated for further analyses.

Video 1.mp4

PLP 136-150

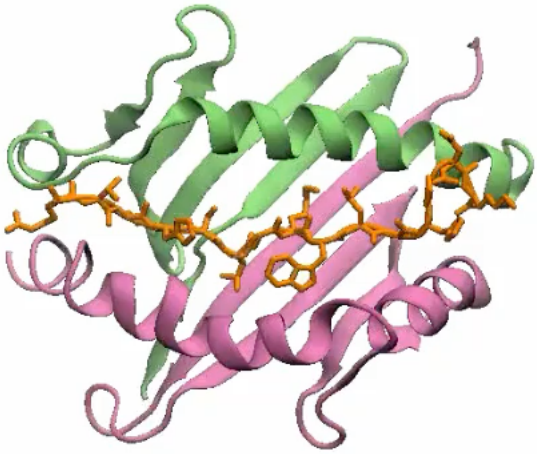

PLP 139-151